

MASTER

Development and characterization of 3D-printed soft gripper

de Groof, R.H.J.

Award date:
2021

[Link to publication](#)

Disclaimer

This document contains a student thesis (bachelor's or master's), as authored by a student at Eindhoven University of Technology. Student theses are made available in the TU/e repository upon obtaining the required degree. The grade received is not published on the document as presented in the repository. The required complexity or quality of research of student theses may vary by program, and the required minimum study period may vary in duration.

General rights

Copyright and moral rights for the publications made accessible in the public portal are retained by the authors and/or other copyright owners and it is a condition of accessing publications that users recognise and abide by the legal requirements associated with these rights.

- Users may download and print one copy of any publication from the public portal for the purpose of private study or research.
- You may not further distribute the material or use it for any profit-making activity or commercial gain

Development and characterization of 3D-printed soft gripper

Master Program
Research group

Mechanical Engineering
Microsystems

Supervisor Holst Centre
Supervisor Holst Centre
Supervisor TU/e

Peter Zalar
Edsger Smits
Jaap den Toonder

Student Name
Student Number

Roel de Groof
0913359



Abstract

This research aimed to develop a multiple degree-of-freedom soft gripper with a single tethered connection. A monolithic soft gripper has been developed using 3D-printing. Soft grippers are necessary when delicate objects with unknown dimensions have to be transported. Soft grippers are able to adjust their shape and therefore prevent local stress concentrations in the object. This research demonstrates the functionality of the gripper by showing the ability to pick five different objects. The developed soft gripper is able to pick up and hold spherical and cubical shaped objects with sizes from 4 to 8 centimeters with masses from 3 up to 583 grams.

In order to investigate the effect on both exerted force and no-load deformation, the design parameters are analyzed individually. The design can be adjusted based on the properties of the object to be grabbed which results in a wide range of possible applications.

In order to create multiple degree-of-freedom actuation of the gripper, this research developed a monolithic valve of the same material as the gripper. This monolithic close-off valve is normally opened and shows the ability of closing a pressurized system that exceeds the threshold of 0.5 bar. This valve is a proof of concept for further investigation of monolithic elastic valves.

Contents

1 Introduction	3
1.1 Goal, design requirements and research questions	4
2 Background	5
2.1 Additive manufacturing methods	5
2.2 Published research for soft grippers	7
2.3 Advanced actuation	9
3 Methods	12
3.1 Printability	12
3.2 Material properties	14
3.3 Development of gripper	19
3.4 Design parameters	19
3.5 Valve development	24
4 Results	26
4.1 Printability	26
4.2 Material properties	28
4.3 Soft grippers	34
4.4 Gripping demonstration	44
4.5 Valve	47
5 Conclusions	51
6 Future research	53
6.1 Soft gripper design	53
6.2 Implementation of strain sensors	53
6.3 Advanced actuation	55
A Appendix	56

1 Introduction

TNO is an independent research organisation that connects people and knowledge to create innovation, which increases the well-being and competitiveness of companies. In cooperation with imec, TNO has founded an open innovation research center called Holst Centre, which is located in Eindhoven on the High-Tech Campus. Holst Centre focuses its research on the mobility, energy, health, and vitality markets. The research fields of Holst Centre are thin-film technology, sensor technology and hybrid printed electronics. Holst Centre is interested in integrating sensing abilities in a wide range of objects.

At commercial production sites, objects have to be moved from one place to another. The common method for this movement is to grab the object using a mechanical robot arm. If the object properties such as shape and stiffness are known, using a stiff robot arm is a very powerful method of grabbing objects. A problem occurs when the exact size and shape are unknown. Programming these grippers is difficult when no feedback mechanism is present, e.g. strain or force feedback. For instance, if a stiff gripper is used to grab fruits, which vary in size, the gripper will crush the fruits rather than pick them up and leave them intact. A solution to overcome this problem is to use soft grippers.

Soft grippers are defined by Shintake et. al. (2019): "Soft grippers integrate underactuation and compliance by replacing rigid joints with a structure made of hyperelastic materials that deform continuously in response to external or internal actuators and to the interaction with the objects" [1]. In other words, the gripper is soft and will adjust its shape to the object it is grabbing. As a result, the use of soft grippers reduces the probability of creating local stresses in the object significantly. To conclude, soft grippers create a firmer grip without increasing the stress on the object, which reduces the probability of damaging the object.

The common production technique for soft grippers is the casting and molding method [2-5]. It is easy to use, however it is limited in design of the product [6]. In addition, poor control of this method causes failures such as undesired air bubbles being formed during casting. Furthermore, the object may rupture during demolding due to undesired adhesion to the mold.

Soft grippers require external driving force to be actuated. Soft grippers can be actuated by mechanical, pneumatic or hydraulic forces. Using mechanical actuation requires complex structures due to internal mechanical pushing or pulling. During operation or preparation of a hydraulic gripper, liquids may be spilled. Pneumatic actuation has no spillage and the object does not require parts to be assembled, therefore pneumatic actuation is the preferred driving force. The device that is pneumatically actuated requires cavities to transport air resulting in complex structures of soft grippers. If such complex internal geometries are required, production is costly in terms of labour. The casting and molding method consists of: 1. producing a mold for each layer of the design, 2. pouring the material in the mold, 3. aligning and bonding the layers to create the device. The fact that the final object should be built from multiple layers limits the design possibilities for a gripper tremendously. Using the casting and molding method, the designer is bound to quasi-3D structures.

One solution to overcome the described limitations to complex geometries is to use Additive Manufacturing (AM). Affordable 3D-printers are available on the market for a couple of years at the time of writing. The limiting factor for soft robotic applications is the availability of elastic and printable materials. At the start of the year 2019 Formlabs presented 3D-printable elastic material with promising properties [7, 8]. The chemical composition of this Formlabs Elastic 50A material has not been publicly presented by Formlabs. The Elastic 50A resin has a high solubility in isopropanol alcohol, which can be concluded from the post-processing treatment advised by Formlabs. In addition, the material will cure after UV light and temperature treatment.

1.1 Goal, design requirements and research questions

The goal of this project is to develop a 3D-printed soft gripper, test its functionality and determine how design parameters can be modified to a specific application. The additional goal is to develop a valve that is able to add functionality to this gripper by creating advanced actuation possibilities. To achieve this goal, research questions and design goals are defined below.

The general requirements for the gripper are defined such that it is in line with a variety of objects which are present in e.g. production industry, as well as in fruit harvesting industry. The gripper should be able to pick up objects with the following properties:

- size up to 10 cm
- mass up to 500 grams
- different shapes, spheres and cubes

General research questions to be answered

- What are the mechanical properties of the materials after printing?
- What are the size limits of printing small channels, i.e. the size of the smallest printable channel?
- What are the possibilities for multimaterial printing such that channels can be filled with conductive ink, liquid metal or conductive hydrogels?
- What are the design rules for robust printing?

Specific research questions of soft gripper development to be answered

- What is the advantage of 3D-printing over casting and molding for soft grippers?
- How can a more complex geometry of a soft gripper increase the universal grabbing abilities?
- Can the gripper pick up complex geometries and sizes with a mass up to 500 grams?
- How is the gripper functionality affected by changing geometrical parameters?
- Is it possible to create a one-part soft gripper with multiple degrees of freedom while having a single actuator?
 - What are the possibilities regarding the integration of valves into a gripper?
 - What is the capacity of printable valves with respect to pressure directing/regulating?

The remainder of this report comprises the following: background, methods, results, conclusions and recommendations. In [Section 2](#), published literature will be presented focusing on soft grippers and valves. In [Section 3](#), the methods will be described, i.e. what research methods are used, how measurements are executed and how data are analyzed. In [Section 4](#), the obtained results will be presented and analyzed in depth to be able to draw a substantiated conclusion in [Section 5](#). Recommendations for future research are presented in [Section 6](#).

This project is executed as a graduation project for the master Mechanical Engineering, at the research group Microsystems at the Eindhoven University of Technology. The purpose of the microsystems research group is to develop innovative technological concepts and fabrication methods, for microsystems for a wide range of applications. One of the focus point of this project is the investigation of the spatial limits of several additive manufacturing methods. This project is therefore aligned with the interest of the microsystems group.

2 Background

In this section the relevant published research is presented. First, the considered additive manufacturing (AM) methods are described, subsequently publications of soft grippers and valves actuation principles are presented.

2.1 Additive manufacturing methods

For production of soft grippers, fused deposition modelling (FDM) and stereolithography apparatus (SLA) printing are considered as the most promising methods. FDM has been used widely in literature which will be presented below. As seen in [Figure 1](#), SLA shows the combination of low tensile modulus along with decent ultimate elongation, therefore SLA shows promising material properties. Holst Centre provides the machinery for both AM methods.

Fused deposition modelling

Fused deposition modelling (FDM) is a commonly used AM method. Quality tabletop FDM printers can be purchased for less than €1000, without the need for additional post-processing machinery. The working principle of the FDM printer is based on melting a thermoplastic polymer. The principle of FDM is that the polymeric filament is pushed through a nozzle with a temperature of approximately 200°C, onto a heated bed of approximately 60°C. These are reference temperatures which differ per material and even per printer. During the printing process the filament is melted, from which line by line and layer by layer a structure is built when the material solidifies on the printing bed. This method is schematically visualized in [Figure 2a](#).

FDM printable polymers are mostly stiff or flexible, but never stretchable, as stated by Keneth et. al. (2020) [\[10\]](#). However, recently filaments have been introduced to the market which show stretchable properties. The filaments are introduced by NinjaTek with the NinjaFlex TPU filament and by Recreus with the Filaflex filament. Due to the stretchable properties of the filament, these materials are significantly more difficult to print properly. Most flexible filaments are made of Thermoplastic Polyurethane (TPU), in contrast to stiff filaments which are primarily made of PLA, ABS and PETG.

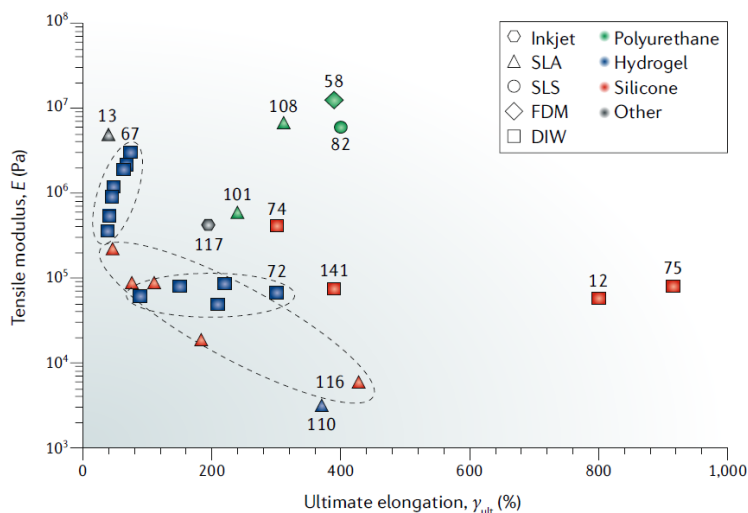


Figure 1: Tensile modulus and ultimate elongation values shown for several AM methods combined with the corresponding material [\[9\]](#).

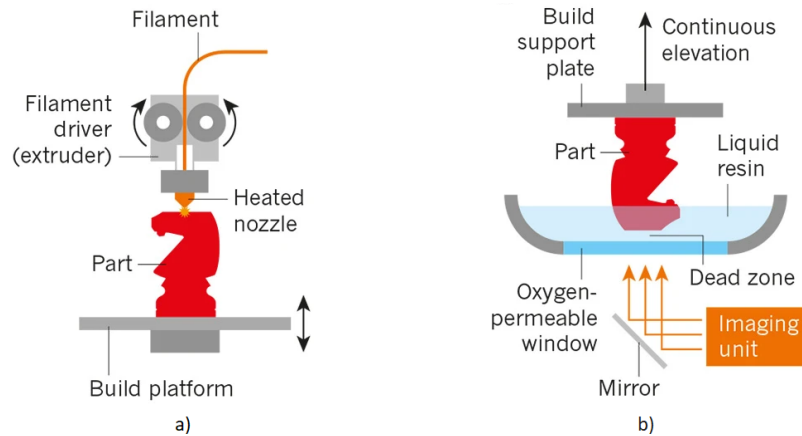


Figure 2: Two schematics of additive manufacturing methods: a) FDM, b) SLA. FDM method based on extrusion of a thermoplastic filament. SLA printing based on curing photosensitive resin onto a submerged build platform and previous layers [17].

Each AM method has advantages and disadvantages. The FDM method has been widely used to, amongst others, develop molds for the molding and casting method, and for the production of the body of a soft gripper [11-15]. The advantage of FDM is the affordable machinery and materials. However, the disadvantage is that the printing process creates voids and defects. The hydrophilic property of FDM filament absorbs moisture from the air, consequently causing voids and defects during printing of the filament. Therefore, thick walls are required to ensure full air tightness. In addition, very flexible materials or material with high transition temperatures are difficult to print properly [16].

Vat polymerization

The second investigated AM technique is the vat polymerization method. The general principle of vat polymerization printing is a build platform being submerged in a resin bath, after which a single layer is cured onto the previous layer on the build platform. The general method can be subdivided into the following single methods: stereolithography apparatus (SLA), digital light processing (DLP), light crystal display (LCD), continuous liquid interface production (CLIP) and two-photon polymerization (2PP) [9]. The primary distinction between these single methods is the way of curing the material in a single layer. Due to availability of machinery at Holst Centre, the SLA method has been further investigated.

The stereolithography apparatus (SLA) printing method is illustrated in Figure 2b. The build platform which faces down, is submerged into a resin bath to the height of a single layer ($100\ \mu\text{m}$) above the bottom. The bottom of the bath is a foil which allows the laser to pass through. The liquid resin between the build platform and the foil is cured by a single point laser that scans the surface pattern that needs to be cured for the first layer. Since the material is cured onto the foil, a peeling movement is made to peel the foil off the material to minimize the forces on the object. At this point the first layer is completed, after which the build platform rises out of the resin bath. The build platform will again lower into the bath, such that the distance between the previously created layer of material and the foil, is again exactly one layer height ($100\ \mu\text{m}$). This processes is repeated until a 3D structure is created. After the printed part is finished, the operator should wash off the excessive resin, and post-cure the part using a UV curing machine at an elevated temperature. The full line of quality SLA machinery can be purchased from Formlabs for approximately €4500, including the wash and cure machines.

The disadvantage of this method is the costs of both the machinery and the material. The machinery is five times more expensive than FDM machinery. In addition at the time of writing the material cost are €190 per liter which is approximately two times the cost of FDM material. Another disadvantage is the post processing of cavities. Small cavities are filled with resin after printing, which should be removed before post-curing. The cavities should be designed such that the operator is able to clean excessive resin using solvent. However, these cavities are very difficult to produce using FDM. The primary advantage of vat polymerization is that the printing allows for a very robust printing process while maintaining a layer height of $100\ \mu\text{m}$. The resolution in z -direction is $100\ \mu\text{m}$, and lateral resolution is expected to be below $100\ \mu\text{m}$. Successful printing small features primarily depend on stiffness of the object during printing, rather than the spatial limits of curing. Formlabs is currently developing the printing process further for Elastic 50A resin, focusing on print accuracy, printing times and cosmetic flaws. This is presented in the already available beta version of the printing software. It is therefore assumed that resolution will be increased in the near future.

In terms of material selection, the used resin should hold the following two properties: The resin should have a viscosity below $5\text{Pa}\cdot\text{s}$, and the resin should be photocurable. In 2018, material with compatible properties for soft robotics lacked availability[9]. Yap et. al. (2020), presented several researches into 3D-printed soft robotics, showing that materials are available, but tend to have low ultimate strength and poor fatigue properties[16]. In May 2020, Jan et. al. concluded that existing research on 3D-printed complex geometries is based on custom-made 3D-printers or very expensive machinery[18]. The Formlabs SLA machinery available at Holst Centre is user friendly, but consequently does not allow for custom resin usage, since no cure or flow parameters can be set by the operator. This research project will therefore focus primarily on commercially available and affordable machinery and materials, which is currently provided by Formlabs[8].

2.2 Published research for soft grippers

For the past year, research in soft robotics has been an emerging topic. Therefore the useful results and possibilities that follow from this literature have also been presented over the last couple of years. In this subsection the available research on 3D-printed soft grippers will be presented in chronological order.

Peele et. al. (2015) presented a DLP printed soft gripper, which is produced using commercially available material and machinery[19]. This gripper, shown in Figure 3, has multi degrees of freedom actuation, actuated by multiple tethered connections. The monolithic gripper can be printed in one part and assembly is not necessary. The forces it can exert are depicted in Figure 3b, which is measured up to approximately 0.65 N.

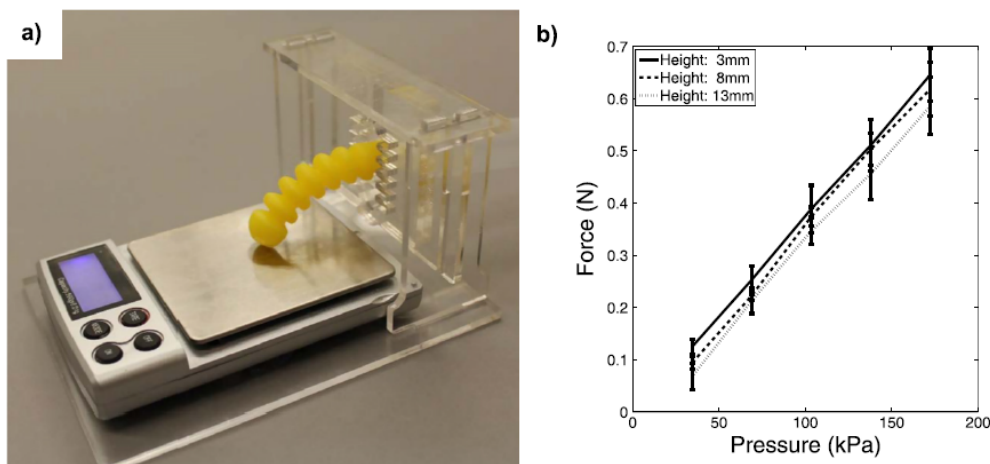


Figure 3: DLP printed soft gripper using commercially available materials. a) force measurement set-up. b) force measurement result as function of inlet pressure[19].

Yap et. al. (2016) presented a FDM printed gripper using commercially available machinery and filaments [13]. This gripper is depicted in Figure 4. The gripper is able to exert high forces such as 70-77 N, even at high pressure up to 300 kPa. However, if low pressure and delicate forces are desired, this gripper is not suitable [13].

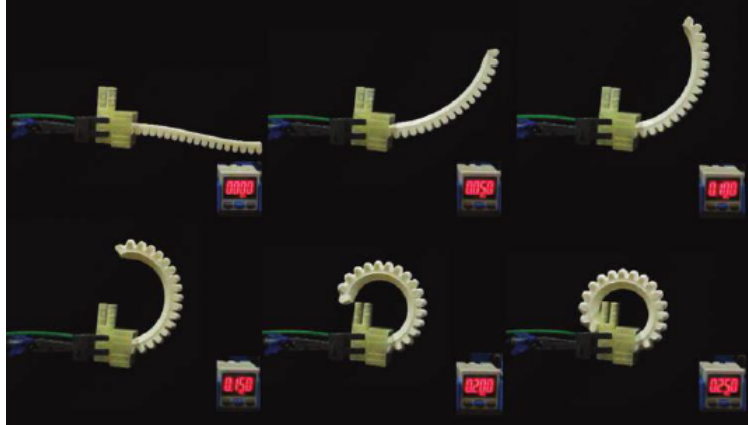


Figure 4: FDM printed gripper presented by Yap et. al. (2016) [13].

Dilibal et. al. (2021) presented a promising FDM printed gripper illustrated in Figure 5 [15]. It is produced by FDM printing a commercial flexible filament, which has a shore hardness of 85A and is made by Shenzhen Esun Industrial Company. The paper lacks of more detailed material information. The designed gripper is able to withstand internal pressures up to 0.8 MPa without leakage and is able to exert forces of up to 8 N on an object as shown in Figure 5. The gripper is able to pick up spherical objects with diameters ranging from 54 to 120 mm.

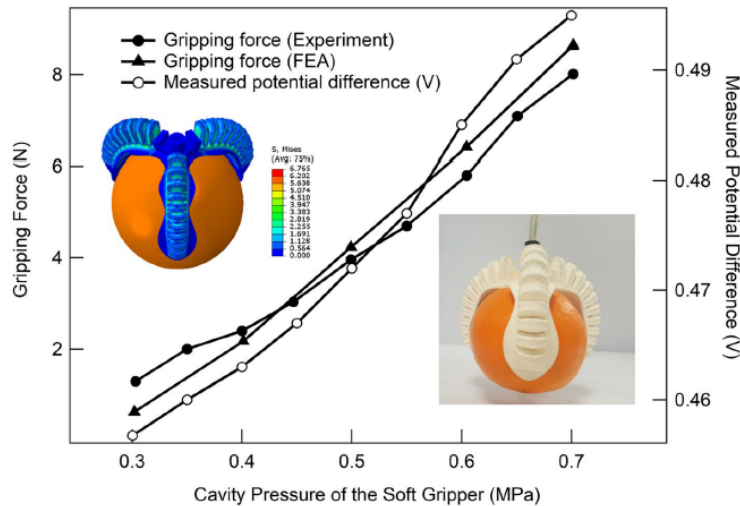


Figure 5: Relation between actuation pressure and exerted forces on the object. Gripper is made by FDM printing a flexible material with integrated force sensor [15].

Many studies of soft grippers are available from the last decade. Nevertheless, there is room for improvement within the existing literature. Dou et. al. (2021) states "The challenges of soft robotic manipulators in terms of materials and structure design, stiffness control, perception, and function control remain to be overcome. [20]". Therefore this research will extend and complement the existing literature, based on different AM methods, by investigating more elastic materials while still assuring easy manufacturing and wide application possibilities.

Commercial soft gripper

In addition to the soft grippers available in existing literature, a soft gripper is available on the commercial market. A soft gripper kit from Soft Robotics Inc. as shown in [Figure 6](#) can be bought from Distrilec for approximately €4100 [\[21\]](#), [\[22\]](#). The reported specifications for a two fingered gripper are: 1. the gripper has a stroke of 100 mm and 2. an operating force of 8 N per finger. The operating range is -0.35 up to 0.7 bar. The gripper consists of a modular mechanical attachment system, which can increase the distance between the fingers by adding spacers. The fingers are expected to be produced by injection blow molding or a comparable production process.



Figure 6: Commercial available soft gripper, developed by Soft Robotics inc., grabbing a nail polish bottle.

2.3 Advanced actuation

Soft grippers are able to adjust their shape to the object due to their low stiffness. In addition, in certain applications it can be useful to have multiple degree of freedom actuation, such as the system presented by Wu et. al. (2019), where the gripper has two individual actuation components [\[23\]](#). In contrast to the design presented in Wu et. al. (2019) it is desired to have only a single actuator attachment in order to prevent superfluous interfacing and bulky equipment [\[24\]](#).

To be able to actuate multiple degrees of freedom using a single actuator, is it required to integrate a method in the device to direct the actuating fluid to the desired location. This can be achieved by using integrated valves, more specific, a monolithic self-actuating valve. This project is about monolithic 3D-printed grippers, therefore integration of valve should also be monolithic. This means no differences in curing times, in contrast to 'monolithic' PDMS devices as seen in Mosadegh et. al. (2008) [\[24\]](#). To actuate the system with only one connection, the valve is required to be passive, which means that the valve should be actuated by properties of the primary fluid flow.

One example of a traditional valve system is presented in Unger et. al. (2000) [\[25\]](#). The presented valve is able to open and close, pump fluid by peristaltic movement and switch direction of fluid. This valve is monolithic, however the disadvantage is the fabrication method which is not compatible with 3D-printing due to the stacking of layers, and more importantly, the valve requires active actuation [\[25\]](#).

Mosadegh et. al. (2008) presented a monolithic and passive valve. The general working can be seen in [Figure 7](#). The type of valve is a check-valve, which allows forward flow of fluid and prevents the fluid from flowing back. The presented valve is an example of how active flow can be utilized. The fabrication method however consists of manual stacking of layers, which is an undesired process.

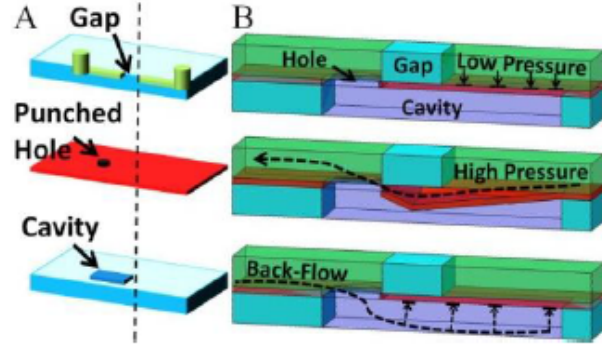


Figure 7: Monolithic passive valve presented by Mosadegh et. al. (2008) [24].

A decade later, Walczak et. al. (2017) presented a valve that eliminates the layered structure, and fabricated a check-valve using 3D-printing. The schematics of the valve are shown in Figure 8. The challenge of 3D-printing is that normally closed valves cannot be printed, since the material will bond during the printing process and will form a solid structure. Therefore a designer remains bound to normally opened valves. This is depicted in Figure 8 in which the valve is not fully closed, whereas in Figure 7 the valve is, as desired, fully closed without any actuation. The Young's modulus of the used material is approximately 500 MPa [26]. The use of 3D-printing provides quick valve production and more complex valve designs can be made [26].

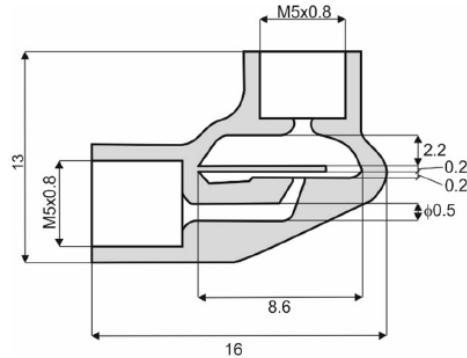


Figure 8: 3D-printed monolithic passive valve presented by Walczak et. al. (2017) [26]. The shown dimensions are in millimeters.

It is shown that 3D-printing can provide very small, lightweight valves which show the ability to be integrated in large devices. Zatopa et. al. (2018) provided an electro-active valve which is able to close and hold against a pressure of up to 264 kPa. The valve of only 10 grams is depicted in Figure 9 [27]. The used material of the valve has a reported tensile strength of 1.9 - 3.0 MPa [28]. This research shows that the need for large rigid valves is eliminated as well as a large number of tethered connections. This is promising research to create soft robotics which are simple, fully soft, and controllable [27]. What needs improvement in the work of Zatopa et. at. (2018) is that an easier manufacturing process is necessary to integrate the valve easily into a gripper.

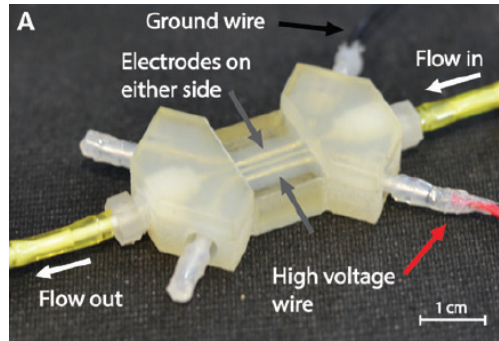


Figure 9: 3D-printed electro-active valve presented by Zatopa et. al. (2017), with a mass of 10 grams and is able to close off a maximum pressure of 264 kPa [27].

It can be concluded from the existing research that a valve which can be implemented in soft grippers is not yet developed. Although the above mentioned literature achieved several of the below mentioned desired properties, a fully integrable solution is still lacking. Ideally a valve should be:

- elastic
- monolithic (including the same curing time)
- small in dimensions (< 1 cm)
- easy to manufacture.

The above stated properties accommodate a valve to be integrated into a gripper without adding complex steps to the production process.

3 Methods

In this section, the experiments that will be executed are explained in terms of methods used and how analyses will be performed. The results of these experiments are subsequently discussed in [Section 4](#)

3.1 Printability

The production method of casting and molding limits the design of the object. Therefore this research focuses on 3D-printing, but 3D-printing has to cope with design limitations as well. For instance, limitations such as the smallest size of design features, as well as the necessity to clean uncured resin out of cavities. These factors are investigated with focus on application of a pneumatic gripper.

Formlabs reports the following print parameters for the Elastic 50A material:

	Minimum [μm]	Maximum [μm]
Supported wall thickness	400	600
Unsupported wall thickness	600	800
Shallow angles	19°	45°
Horizontal span/bridge	-	600
Vertical wire diameter	300	1500
Clearance between adjacent parts	1000	-
Hole diameter	800	-

Table 1: Reported design and print parameters for the Elastic 50A material reported by the manufacturer Formlabs [29](#).

Some parameters are in practice more complex than solely a value for a hole diameter. Important questions are firstly, whether the minimal channel diameter is dependent on orientation. Secondly, the minimal dimension for printing robust walls depending on varying design cases needs to be considered. Therefore several unknown parameters will be investigated.

Channels

In order to develop a pneumatic gripper, it is desired that robust constant diameter channels can be printed as small as possible. To obtain knowledge about the limits, a block will be printed with multiple integrated channels. These channels have a diameter dimension of 1 mm to 5 mm, increasing in steps of 0.5 mm. The model can be seen in [Figure 10a](#). The channels can be visually inspected after printing and we will observe whether each channel has a constant diameter without local narrowing. This block with multiple diameter channels will be printed in both horizontal and vertical print orientation, in order to gather information on directional print dependency of channels.

Subsequently to the diameter analysis, a curved channel is printed as depicted in [Figure 10b](#). In addition to a channel with the minimal robust printable diameter of the previous test, the channel contains an angle of 90°. The radius of the curvature is varied from 1.5 mm to 7.5 mm in order to investigate whether a minimal curvature radius is necessary to prevent channel blockage.

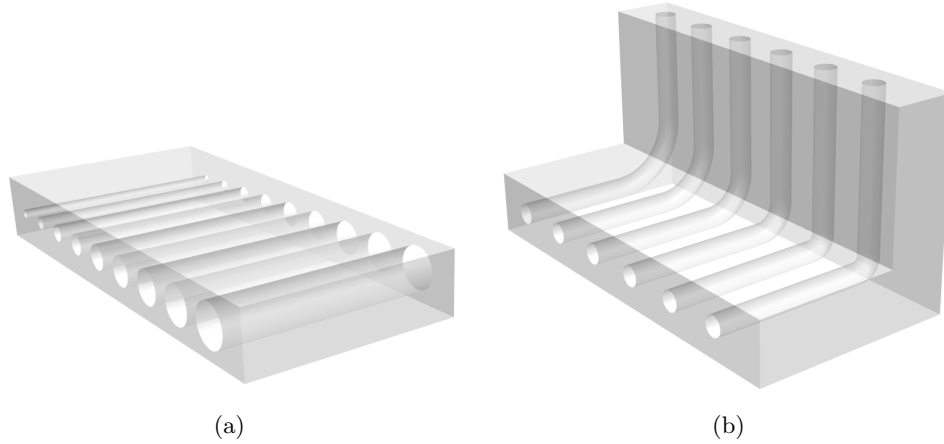


Figure 10: a) Block with channels with diameter 1 mm up to 5 mm with steps of 0.5 mm. b) Channels containing curvature with radius of 1.5 mm up to 7.5 mm.

Hollow structures and cavities

After printing, cavities in the printed object may be filled with undesired resin. Before post-curing an object, the resin has to be extracted from the parts cavities, otherwise this results in the undesired resin to be cured. Therefore, it is interesting to investigate the possibility of printing hollow structures without the need to extract excessive amounts of resin, since this is costly in operator labour time.

To obtain knowledge about the printing behavior of these cavities, multiple closed hollow structures are printed such as a pyramid, a bowl and a cone. First, these shapes are printed with a height of 1 cm, for which it is expected that undesired resin will be encapsulated. The size of the testing shapes are subsequently increased to match the gripper balloon size. It is expected that the amount of encapsulated resin will significantly decrease when the object size increases.

3.2 Material properties

Knowledge about the behavior of the material is necessary for designing a functional device. We are interested in how the material elongates and how it compresses after elongation. Therefore the interesting parameters are tangent modulus, Young’s modulus, hysteresis and ultimate elongation. The material has to be measured while considering practical operation parameters such as speed. Assumptions have to be formulated for measurement parameters such as strain rate.

The material parameters as reported by the manufacturer are stated in [Table 2](#)

Table 2: Reported material parameters of the Formlabs Elastic 50A material [\[29\]](#).

Parameter	Reported value
Shore hardness	50A
Ultimate elongation	160%
Tensile strength	3.2 MPa
Tear strength	19.1 kN/m

Shore hardness is the accustomed parameter used by retailers to present the elasticity of a material. The shore hardness is defined by the indentation depth at a specific force and a specific indenter, which are defined by the durometer scale, in this case: scale A. This experiment results in a value for local compression rather than for global elongation. These two parameters are related but not interchangeable. Therefore, the shore hardness will be rejected as a suitable parameter and experiments will be executed to gather information on the global elasticity of the material. To determine the strain behavior, the Young’s modulus will be determined. In addition, to gather information on how the resistance to strain changes at higher values of strain, the tangent modulus will be determined. Since the gripper will operate in the large strain regime, the tangent modulus is of interest.

From the same measurement data, hysteresis will be analyzed. Hysteresis is defined as the difference in measured values of loading in one direction, compared to the values of loading in the other direction, in this case loading and unloading. Hysteresis may be caused by viscoelastic effects of the material. Hysteresis is measured as a percentage, calculated by the difference in y-values at the center of the x-range divided by the total range of y-values:

$$\text{Hysteresis}\% = |(y_{mid,high} - y_{mid,low}) / (y_{max} - y_{min})| \cdot 100\%. \quad (1)$$

These measurement data are obtained using a tensile test. Dogbone shaped specimens are used in these experiments to prevent clamping effects. A geometrical compensation for this dogbone shape will be discussed later this section. The load cycle of the measurement is displacement controlled with a strain rate of 20 mm/min, which is relatively slow but a realistic value for regular operation of a soft gripper. The load cycle is defined in steps: load, pause 5 seconds, unload, pause 5 seconds, next cycle. The extension is presented in engineering strain ϵ_{eng} , which is defined as the increase in length relative to the initial length. This will further be discussed in [Subsection 4.2](#). The load cycle is depicted in [Figure 11](#) and:

- load to $\epsilon_{eng} = 0.05$
- pause 5 seconds
- unload to $\epsilon_{eng} = 0$
- pause 5 seconds
- load to $\epsilon_{eng} = 0.1$
- pause 5 seconds
- unload to $\epsilon_{eng} = 0$
- pause 5 seconds

- load to $\epsilon_{eng} = 0.2$
- pause 5 seconds
- unload to $\epsilon_{eng} = 0$.

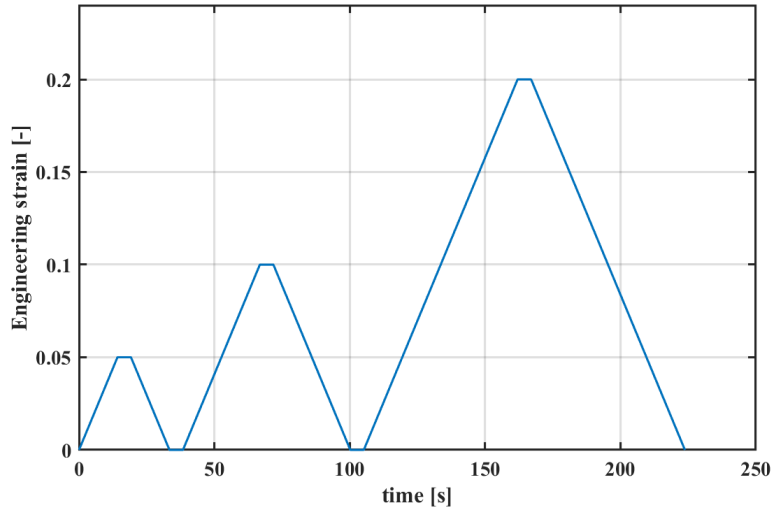


Figure 11: The strain controlled test sequence for determining hysteresis and elasticity.

Specimen geometry

During the tensile test, large forces are exerted on the specimen. It is therefore necessary that the specimen is clamped tight in the measurement tool. This clamping pressure induces stress around the clamping location in the specimen, which influences the measured data. To prevent this induced stress from being significant, dogbone shaped specimens will be used. The shape and dimensions of the specimen are visualized in [Figure 12](#).

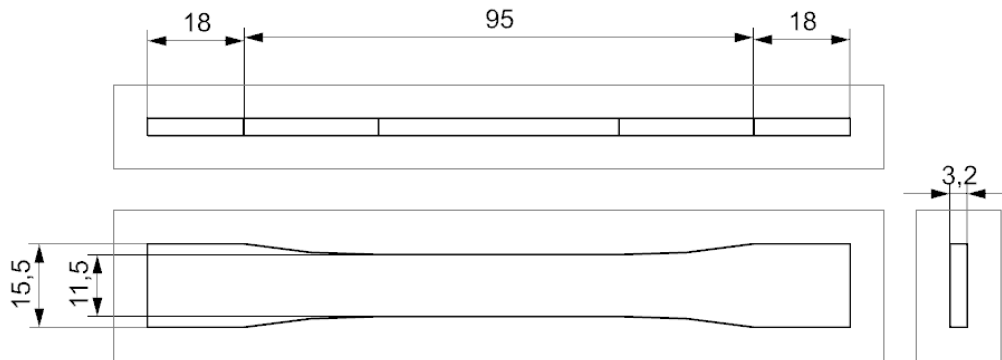


Figure 12: Technical drawing of dogbone specimen, measurements are in [mm].

The middle section of the specimen is the region of interest for further analysis. Since the specimen is measured globally, also the wide part of the specimen is strained and therefore measured. Close to the clamps, the specimen is wider which results in more strained material. Since this excessive material will influence the global strain behavior, the raw measurement data have to be compensated for this non-uniform geometry. The total measured elongation should be scaled with a constant factor which is only dependent on geometry. This factor is calculated by dividing the specimen length L into multiple elements of length dL , where $dL \ll L$. Since the strain in the specimen can be assumed to be a system of elements in series, the stress in every element is equal. For an arbitrary value of the Young's modulus and applied force, the local engineering strain is calculated using:

$$\epsilon_{local} = F \cdot dL / (A_{local} \cdot E). \quad (2)$$

Where A_{local} is the local cross-sectional area, E and F arbitrary values for Young's modulus and force, and dL the length of the element. It is expected that for each element with the same cross-sectional area, ϵ_{local} is constant, which is in line with the relation shown in [Equation 2](#). Consequently global strain is calculated using:

$$\epsilon_{global} = \sum_{i=0}^L \epsilon_i(dL). \quad (3)$$

The global strain will be measured during the experiment and we are interested in the local strain at the middle section. The compensation ratio is therefore defined as:

$$\epsilon_{ratio} = \epsilon_{local} / \epsilon_{global}. \quad (4)$$

This compensation is based on assumptions which do not hold for the non-linear relation of true strain, therefore this compensation is applied to the engineering strain before conversion to true strain, using:

$$\epsilon_{true} = 1 + \ln(\epsilon_{eng}). \quad (5)$$

When raw data without geometric compensation are used for calculations, the dogbone specimen will appear to have a higher stiffness compared to a simple bar shaped specimen. The bar shaped specimen has the equal dimensions as the dogbone specimen, except for the lack of the increased width at both ends. In other words, the middle sections have equal width. For both geometries, three specimens are tested to verify the presented compensation. The results will be presented in [Figure 24](#) in [Section 4](#).

Measurement equipment

The system that will be used for these measurement is the Instron 5566. The Instron is available at Holst Centre and allows for operation of the aimed experiments. The Instron equipment is depicted in [Figure 13](#) and includes a manual control panel, lower clamp, and a load cell with the upper clamp attached. The load cell and upper clamp are mounted on the traverse which can move up and down. This movement can be controlled using the manual control panel, but also using the software on the attached PC. Using the software, the operator programs the experiment which is subsequently executed by the machine.

The experiment settings consist of:

- Control parameter (strain)
- Strain rate (20 mm/min)
- Load cycle (see [Figure 11](#))
- Output parameters (specimen label, force [N], displacement [mm])

The noise level of the load cell is 10^{-5} times the maximum load, which equals 0.01 N for the 100 N load cell. The position accuracy of the Instron is up to ± 0.02 mm or 0.05% of the displayed reading [\[30\]](#).

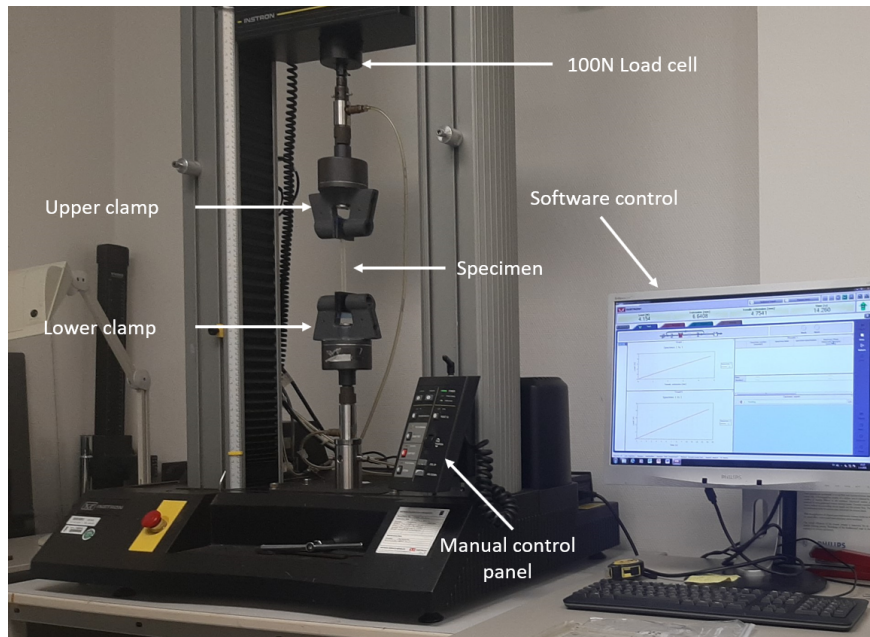


Figure 13: The Instron 5566 measuring equipment with its indicated components.

The measurement data will be visualized in a stress-strain figure. Material properties can be determined from the relation between the stress and strain, for which a schematic example is shown in [Figure 14](#).

Elasticity

One of the parameters that will be obtained from these tensile tests is the elasticity of the material. The elasticity of the material at a certain strain is defined as increased stress induced by a unit of increased strain. By this definition, this is equal to the slope of the stress-strain curve, as visualized in [Figure 14](#). To determine the Young's modulus, the slope of each individual curve has to be determined. The slope is analyzed by a linear approximation of the first 5% of the largest loading cycle. Since for each specimen the Young's modulus is determined, the mean value and the 95% confidence interval can be calculated.

To obtain one representative stress-strain curve for the set of specimens, the individual data sets are interpolated. Interpolation allows for obtaining stress data for all data sets at specified strains, which allows for the individual interpolated stress-strain curves to be averaged. To gather information on how the material behaves at large strains, solely determining the Young's modulus is not sufficient. Therefore, the tangent modulus for the full strain range of the averaged stress-strain curve will be determined.

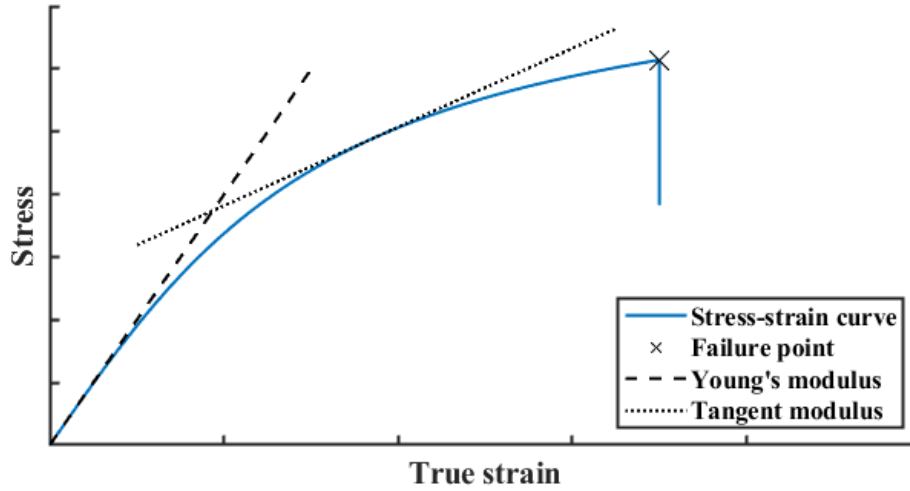


Figure 14: Typical stress stress curve for brittle elastic material. Indicated are the tangent at zero strain which is defined at the Young's modulus, as well as the tangent at an other arbitrary point which is defined as the Tangent modulus for this particular point. The point of failure is indicated which corresponds to the ultimate strain.

Ultimate elongation

In addition to the elastic behavior, we investigate the ultimate elongation property of the material. This material property is analyzed using generally the same method as described previously. The primary difference is that instead of the cyclic measurement, the specimen will be elongated with constant strain rate until the specimen shows instant failure. The strain will be analyzed at the point of break, which is indicated in [Figure 14](#). To be able to present substantial values for ultimate strain, multiple specimens have to be tested. A total of 24 specimens will be tested and analyzed. During testing, visual inspection is executed on what principle the material fails, and the failure location.

Error analysis

When data are presented using a mean value for a set of data, an indication for the distribution of the data points has to be presented. The standard deviation is a indication for variability of the data from the presented mean value. Since we investigate a sample rather than the full population, the standard deviation is calculated by:

$$\sigma = \sqrt{\frac{\sum(x - \bar{x})^2}{n - 1}}. \quad (6)$$

The standard deviation is used to calculate the 95% confidence interval (CI). The 95% CI is defined is 2σ , and data will be presented as $\bar{x} \pm 2\sigma$. The data presented in [Section 4](#) shows the mean of the obtained data, along with the variability such that we can conclude that we are 95% confident that the mean value of the true population lays within this range.

The obtained ultimate elongation data will be analyzed using a Weibull distribution function. This function is applicable to non-normal distributions, for instance of material strength. The three-parameter Weibull distribution function is defined in [Equation 7](#).

$$f(t) = \frac{\beta}{\eta} \left(\frac{t - \gamma}{\eta} \right)^{\beta-1} e^{-\left(\frac{t-\gamma}{\eta}\right)^\beta}, \quad (7)$$

where

η = scale parameter

β = shape parameter

γ = location parameter.

The scale parameter is the maximum of the probability curve, or characteristic ultimate elongation, the shape parameter determines the width of the distribution, and the location parameter is the failure free ultimate elongation. For material properties the characteristic ultimate elongation and the failure free ultimate elongation parameters are important and will be discussed in [Section 4](#)

The parameters are determined utilizing the built-in Matlab functions ‘adtest’ and ‘wblfit’. Adtest will be used to determine the γ parameter since wblfit allow for only the two-parameter Weibull fit. Iteratively, the γ parameter will be determined for which adtest function results in the highest confidence that the data can be described using Weibull fit. Consequently, the wblfit will be utilized to determine η and β parameters for the Weibull distribution.

3.3 Development of gripper

When the printing process is analyzed and the material properties are known, a soft gripper can be designed. Literature shows multiple actuation principles for soft grippers. The optimal actuation principle depends on printability and functionality. It is desired to be printed with minimal post-processing. In addition, the gripper should function using low actuation pressure of below 1 bar, while maximizing the exerted gripping force.

Two designs will be considered: a straight bar with connected compartments and the separated balloon type as seen in [Figure 15a](#) and [15b](#), respectively. A prototype for each concept will be printed and inspected in terms of printability and functionality. Based on the results of this prototyping test, one of these actuation concepts will be used for further investigation.

Design iterations

The grippers are costly in terms of materials, therefore one of the design goals is to minimize material usage. A simple single gripper finger will be printed and subsequently we will inspect where extra rigidity is necessary. The first printed model is seen in [Figure 16](#). This model will be improved on multiple aspects, which will be discussed in [Section 4](#). These iterations are based on providing a general functional gripper rather than the application to a specific object.

3.4 Design parameters

To be able to obtain design rules for grabbing a specific object, the gripper will be tested on functional dependency on various geometrical parameters. These parameters will be tested on both exerted force and zero-load deformation depending on actuation pressure. The tests are all based on a single parameter that deviates from the reference design. The reference design is shown in [Figure 17](#). Four dimensions of the grippers are varied:

- Reference dimensions
- Balloon height
- Balloon wall thickness
- Bottom thickness.

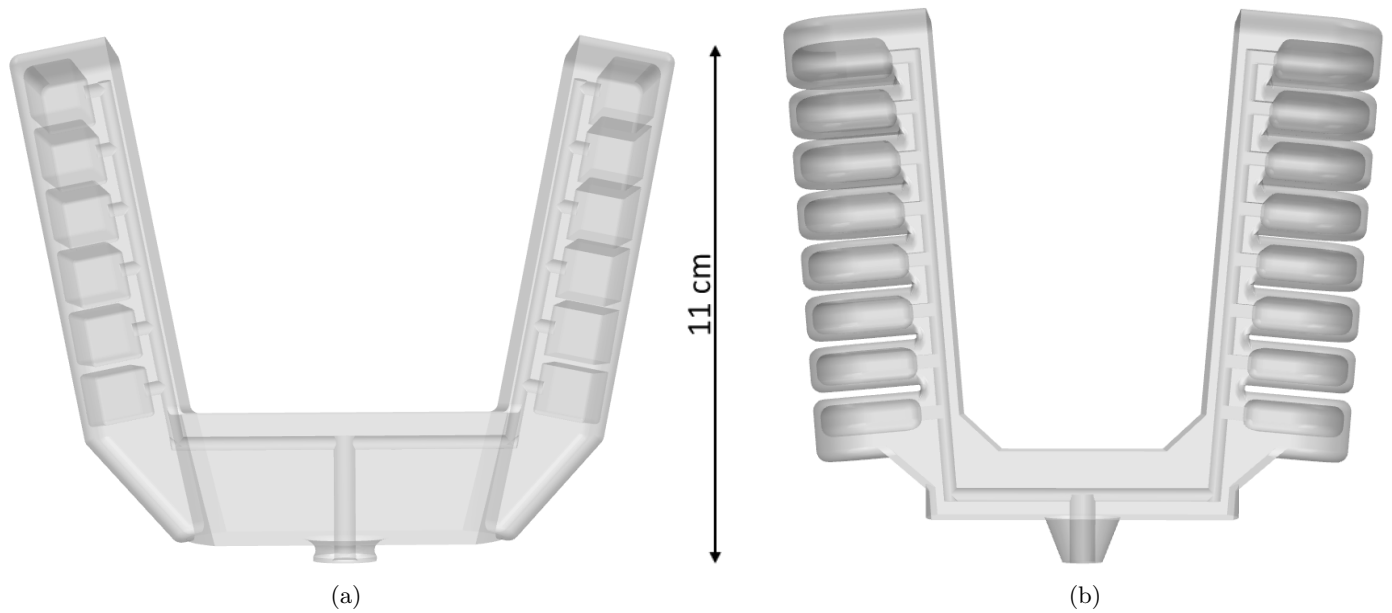


Figure 15: Two considered pneumatic gripper actuation principles. a) Block actuation, in which only internal cavities are defined which by inflation cause bending actuation. b) Balloon actuation, where the inflated balloons press onto each other which causes bending actuation.

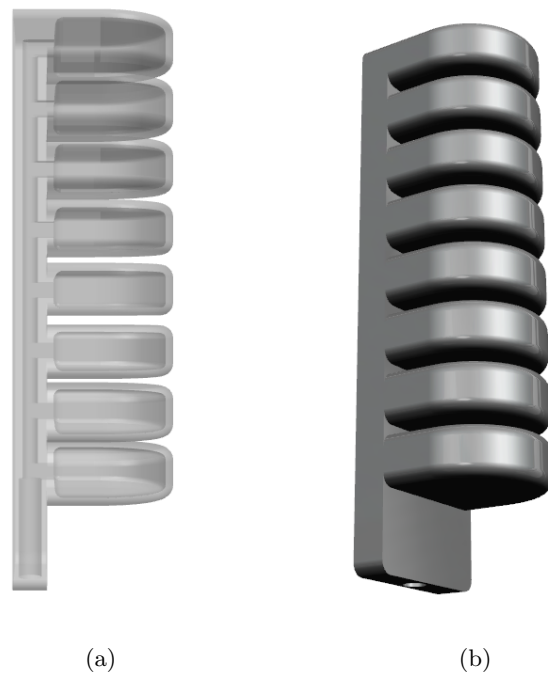


Figure 16: The a) transparent and b) opaque view of the initial prototype design of the single balloon gripper.

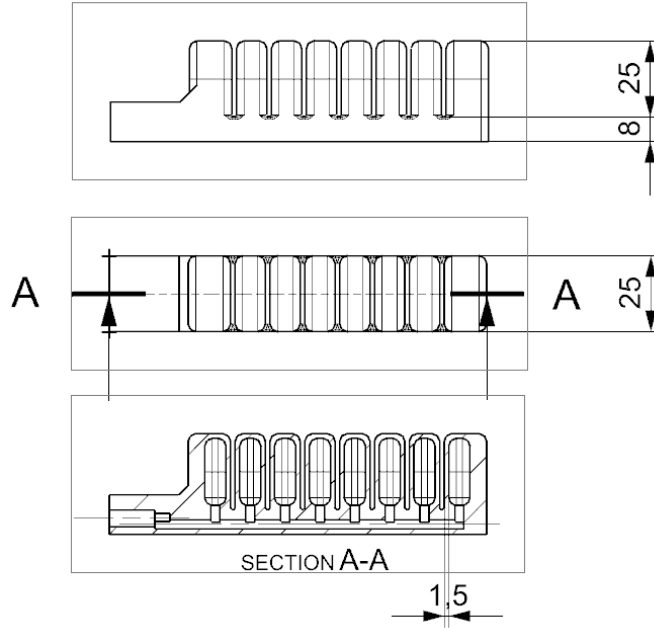


Figure 17: Technical drawing of the single reference gripper. Reference dimensions are shown in millimeters.

The dimensions of the reference grippers are shown in [Figure 17](#). Furthermore, in [Table 3](#) the dimensions that will be tested are shown. For each dimension, three points or data sets are obtained, to be able to draw conclusions in [Section 4](#). To test the repeatability of the printing process, the reference gripper is printed twice and both grippers are tested by executing the same experiment. In addition, the repeatability of the measurement is verified by testing both reference grippers three times.

Table 3: Parameters for testing geometrical dependency of single gripper.

Dimensions	Reference	Variable 1	Variable 2
Balloon height	25 mm	35 mm	45 mm
Bottom thickness	8 mm	6 mm	10 mm
Wall thickness	1.5 mm	2 mm	2.5 mm

As stated, two measurements are executed: the deformation and force measurement. Both parameters are dependent on inlet pressure, which is actuated using a pressure regulator and a pressure indicator. This is an in-house system developed by Holst Centre which is attached to a metal plate, as shown in [Figure 18](#).

Deformation measurement

For each gripper the deformation measurement will be executed using the set-up depicted in [Figure 18](#). The tape measures are aligned at zero deformation. The inlet pressure will be manually increased in steps. Firstly, the pressure is increased up to about half of the expected pressure range. Secondly, the pressure is gradually decreased back to zero deformation. Thirdly, the pressure is increased again up to the maximum pressure which is expected to be safe, then again back to zero. In this way, hysteresis can be observed, as well as whether hysteresis is present above a certain deformation. The obtained data will be visualized for each gripper by plotting the deformation [mm] against the actuation pressure [bar] in [Section 4](#).

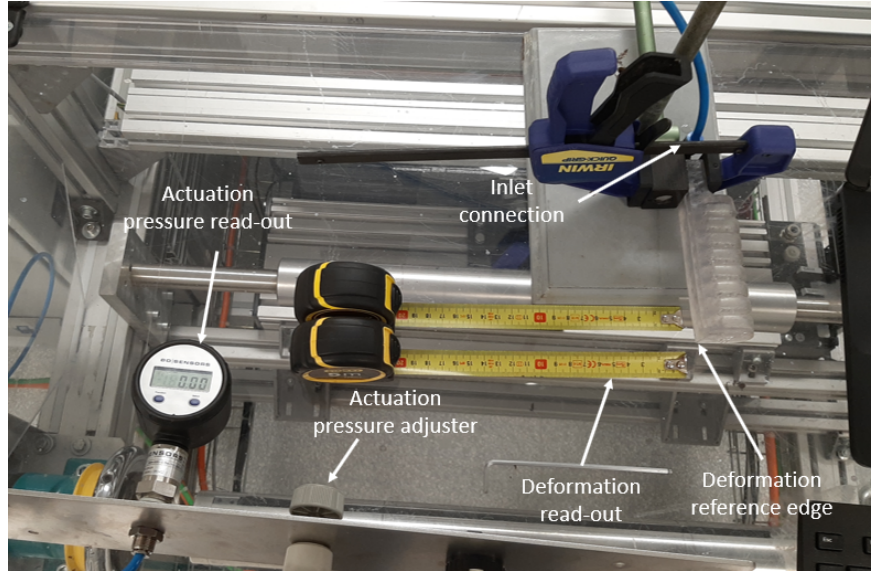


Figure 18: The deformation measurement set-up. On the left the manual input pressure regulating system with a display showing pressure in bar. The gripper is attached to a stand such that the movement is horizontal without any external friction. The reference on the gripper which is measured is the vertical edge.

Force measurement

The force measurement is based on a system similar to the deformation measurement. The gripper is clamped vertically to press onto a load cell, as seen in [Figure 19](#). The inlet pressure is altered as described at the deformation measurement, firstly up to half the maximum pressure, back to zero, secondly up to full pressure, and back to zero. During the initial test measurement, the data showed high values of hysteresis. Therefore a sliding constraint is inserted between the gripper and the load cell. A glass plate is directly attached to the load cell, on which another smaller glass plate is added. By wetting the contacting surface between the glass plates the friction is reduced significantly for the lower range of force, but hysteresis is expected to still be present at higher force since the water is observed to be pushed away.

The gripper exerts force onto a 10 N load cell, connected to a force indicator, the Mark-10 Model 7i. The accuracy of the indicator is 0.1% of full scale, and of the load cell this is 0.15% of full scale [\[31\]](#), [\[32\]](#). Therefore, the global measurement accuracy is 0.25% of 10 N which equals an accuracy of ± 0.025 N.

The obtained data will be visualized for each measurement by plotting the deformation [mm] against the actuation pressure [bar]. These curves are individually analyzed by a linear approximation of the data. The slope of this linear approximation represents the value for dF/dP . These values are depicted to compare the slopes of the curves for each gripper.

Hypotheses

The dimensions of the reference gripper are listed in [Table 3](#). In addition, each parameter stated in the other second and third column are tested individually. Before testing, hypotheses are defined for the expected outcomes of each altered parameter. The outcome of the individual tests are compared to the reference design.

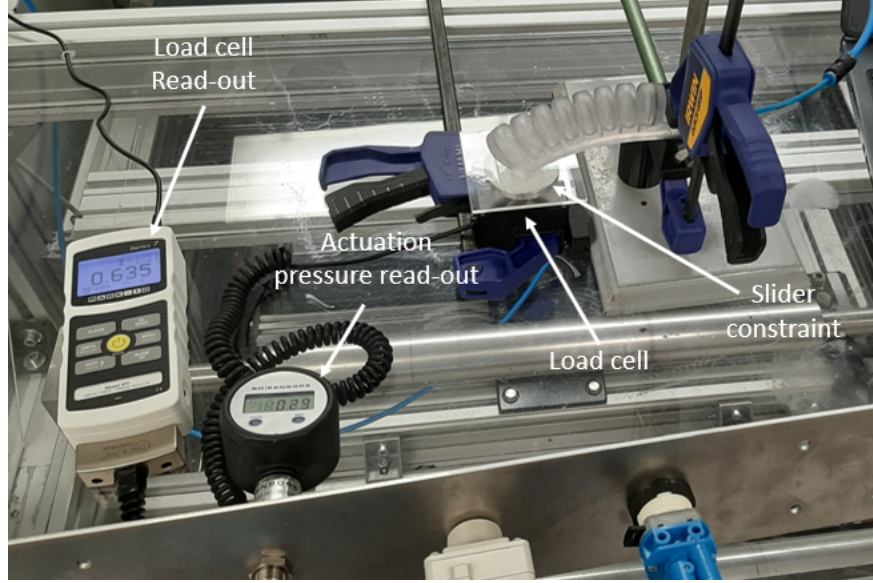


Figure 19: The force measurement set-up. On the left the monitor which is connected to the load cell, from which the force can be read. With the sliding constraint glass plate on top, the vertically placed load cell is depicted on the right.

Wall thickness

When increasing the wall thickness of the balloons, expansion of the balloons require higher pressure, which is a disadvantage. In contrast, we expect that at equal deformation, and thus higher actuation pressures, also higher forces are exerted onto an object. Since force is dependent on the pressure and the surface is by approximation equal, we expect that the forces will increase when operating with higher pressures.

Bottom thickness

The deformation of the gripper is opposed by the bending stiffness of the cuboid shape of the bottom, where the ‘bottom thickness’ is the height of this cuboid. The balloons define a moment parallel to the bottom of the gripper. The opposing bending stiffness can therefore be approximated by single sided clamped beam, driven by a single moment. This is defined for small deflections by:

$$\delta = \frac{ML^2}{2EI}, \text{ where } I = W \cdot H^3/12, \quad (8)$$

where H refers to the bottom thickness, E to the Young’s modulus, M to the moment of force, and L and W to the length and width of the finger [33]. This relation shows that $\delta \propto H^{-3}$. At large deformations, also non-linear effects play a role on the deformation, but since this is too complex to solve analytically for this specific application, low strain approximation is assumed to be sufficient. Therefore, the hypothesis based on this approximation is that the deformation is inversely scales with the bottom thickness cubed. We expect that the force increase per pressure increase is constant, since no geometrical changes are applied to the force generation, namely the balloons.

Balloon height

Increasing the balloon height is expected to significantly influence the generation of forces. The balloons generate a force parallel to the bottom section. This force induces a moment of force on the gripper. We assume that half the balloon height equals the moment arm, schematically visualized by r in [Figure 20](#). Increasing the arm of the moment by increasing the balloon height results in a higher moment of force causing bending of the gripper.

Due to the increase of the balloon height, the area of the expandable side of the balloons is increased. Therefore the balloons will expand more easily which is in addition to the higher moment created by the internal forces. Therefore we expect both the deformation as well as the forces to be increased by an increased balloon height.

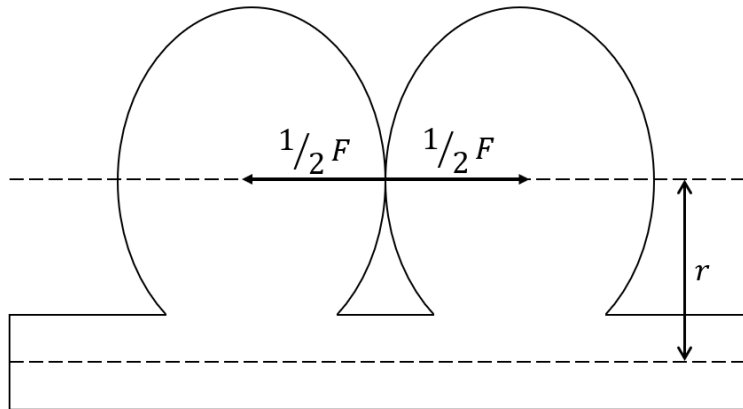


Figure 20: Schematic view of two simplified balloons exerting forces by pushing onto each other. Both balloons experience equal reaction forces, which are parallel to the bottom of the gripper. The distance between these two lines is the arm of moment for the bending of the gripper. The arm r equals approximately half of the balloon height.

3.5 Valve development

To achieve the goal of the advanced actuation, while having a single tethered connection, a complex internal system has to be designed. This complex system should be able to steer, block or access the air at certain pressures. Since the gripper is a one-part 3D-printed object, this complex system should be producible in the same printing process. Therefore, a monolithic 3D-printable valve will be developed.

To develop a full advanced actuating system with one tethered connection, it is necessary to have multiple types of valves. Since the development of a complete set of functional valves is out of scope for this project, we focus on using the printing process for proof of concept for single valve development.

A valve should contain a part that is either able to open and close the main channel or to open and close solely specific channels. When the valve is designed such that it will open in case of actuation, this is called ‘normally closed’. A ‘normally opened’ valve is opened without actuation. When taking into account how the valve will be produced, the valve cannot be normally closed. Normally closed valves require parts touching during production, which is not possible to be printed without bonding onto each other in an AM process. This eliminates the possibility for the valve to be opened. In addition, a pre-loaded structure similar to a spring is necessary to keep the valve closed up to a certain amount of pressure. Due to production limitations, normally opened valves will be further investigated.

Valves are commercially available in mechanical form. These valves are mostly made of metal, and produced and assembled from multiple parts. The functional design of these mechanical valves will be used as inspiration for the design of a monolithic prototype. The first prototype is shown in [Figure 21](#). Further development of this valve and functional testing will be presented in [Section 4](#).

The function of the valve is based on the air pressure that flows through the valve from the inlet to the outlet. When the valve is actuated, the air is restricted from flowing due to the valve stem pulling onto to the valve seat. This movement is created by the pressure that is present at the outlet section of the valve. Here, the air pressure pushes onto the membrane, which deforms the spring-like structure, until the valve stem is pulled onto the valve seat. To limit this movement, and thus to prevent damage to the valve, a depth stop is integrated. The aimed function of this valve is when the pressure increases above a threshold, the valve closes. When subsequently the inlet pressure decreases, the pressure in the outlet and the attached closed system will keep the valve closed, and therefore the system will be kept under pressure, even when the inlet pressure is relieved. Multiple design iterations will be executed based on the presented design. The final design along with the dimensions will be presented in [Section 4](#).

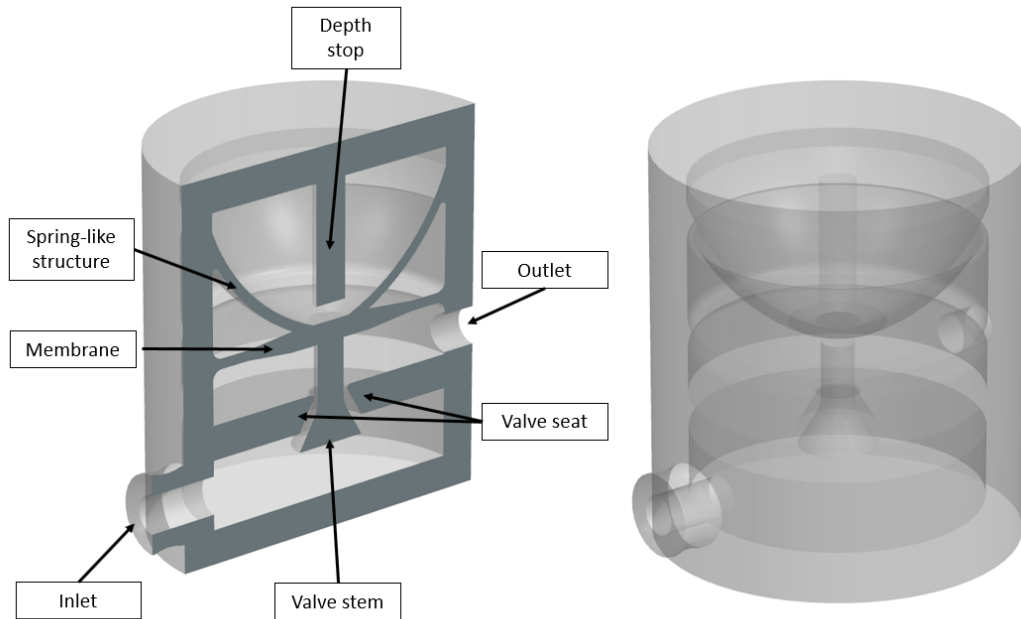


Figure 21: The initial prototype design of the close-off valve. The height of the valve is 55 mm and the diameter is 50 mm.

4 Results

The obtained results are presented in this section in the following order: printability, material properties, soft gripper, demonstration of the gripper, and valve.

4.1 Printability

As formulated by Formlabs and included in [Table 1](#), very specific print parameters are provided. For designing a soft gripper this information is too general and not suitable. Therefore, test prints have been executed to gather information on the ability of the printer to produce a soft gripper. We focused on wall thickness of the balloons, cavities for the pneumatic channels and hollow structures for the balloons.

Channels

The models shown in [Figure 10](#) are printed and inspected, of which the printed results can be observed in [Figure 22](#). In the left figure, both the horizontally and vertically printed channels are depicted. The vertical channels, from 2 mm upwards, show neither blockages nor local narrowing. The horizontal channels, from 2.5 mm upwards, show no blockages however they show some narrowing.

The primary problem with producing these channels is the fact that small channels are difficult to clean. Therefore, if efforts are put into cleaning the smaller channels, these are also printable. As a design rule for the remainder of the project, 3 mm is selected as the minimal channel size. When more complex structures are built, cleaning the channels is even harder to execute properly, therefore 3 mm is considered a robustly printable diameter which provides the operator freedom in terms of design.

In addition, channels with varying curvatures are printed, as depicted in [Figure 22](#)b. Each of the two blocks consists of multiple channels with a constant diameter, 2.5 mm (bottom) and 3 mm (top). Each channel differs in radius of the curvature in the channel, as can be observed in [Figure 10](#)b. We observe no blockage at any curvature radius, therefore it can be concluded that channels of 2.5 mm and larger do not depend on curvature for printability.

Although it is stated that channels greater than 2.5 mm show no blockages, the operator has to manually clean the channels thoroughly before post-curing. If the channels are insufficiently cleaned, it cannot be guaranteed that channels are fully opened independent of the diameter.

Hollow structures

As explained in previous section, hollow structures tend to be filled with resin when the printing process is finished. The operator has to flush channels and cavities, but flushing a whole balloon filled with resin is difficult and expensive in terms of operator time. Therefore it is tested at which size printing hollow structures results in a print that can be flushed without extensive efforts of the operator. Several symmetrical shapes are printed of which cross sections are shown to visualize the inside along with the model in [Figure 23](#). These models are closed and therefore no resin has been flushed, hence this demonstrates the encapsulated resin in a cavity before flushing with solvent.

To be able to extract the resin from a hollow structure a second method was tested. This proposed method consisted of a syringe with a needle, which was used to extract the resin from the cavity. The hypothesis was that the needle perforates the wall of the structure to enter, so it could extract the resin. The wall would be repaired by some resin remains during post-curing which would cure the hole to form a closed system.

In practice, it appeared that the resin was too viscous to be extracted by a needle and a syringe. In addition, due to the absence of post-curing at the time of perforation, the wall had the tendency to rupture. This was the case for wall thicknesses of 1, 1.5, and 2 mm. Therefore this method has been rejected and we continued with flushing cavities using solvent.

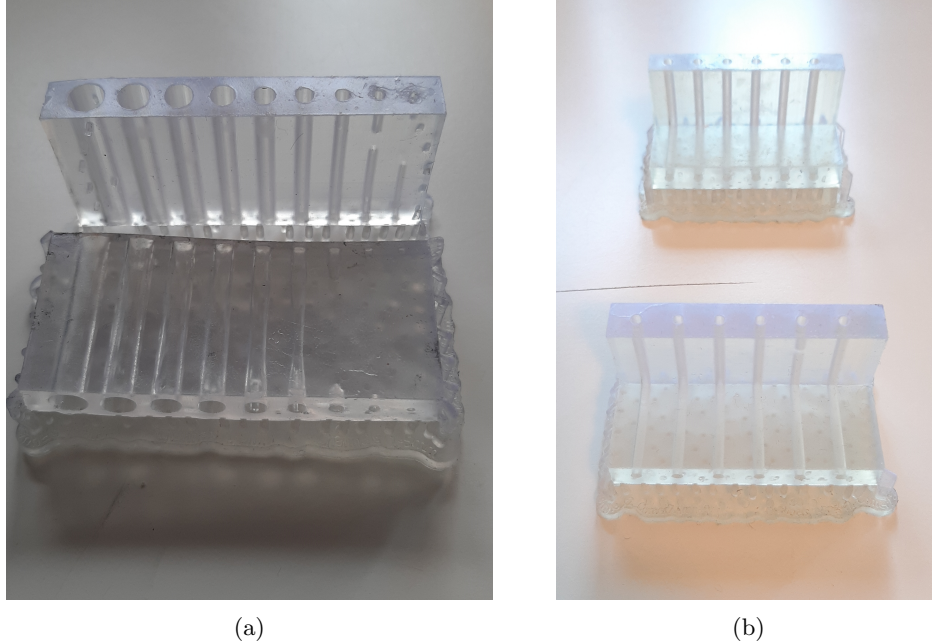


Figure 22: a) Straight channels with diameter of 5 mm (left) to 1 mm (right) with interval of 0.5 mm. Printed vertically (top) and horizontally (bottom). b) Channels diameter of 3 mm (top) and 2.5 mm (bottom). Channels contain a 90° bend with different radii. Radii of 1 mm up to 7.5 mm. No print or cleaning problems are encountered.

These prints were also used to determine robust printable wall thickness. Thickness of 1 mm showed very weak walls in terms of failure during handling, it was observed that the 1 mm thick wall ruptured at connections to for example the bottom section. For 1.5 mm and above, the walls showed fine handling properties without failure.

It is demonstrated that internal flushing is necessary, therefore the hollow structures are increased in size. When the structure has a larger height, it is expected to contain relatively less resin after printing. The amount of resin that is encapsulated during the printing process, is defined by the resin level in the resin tank. To elaborate, due to the fact that the print layer that closes a cavity, is printed at the bottom of the tank above which resin is present, this level of resin will be encapsulated in the object. The larger the height of the printed object compared to the resin level, the less resin is encapsulated relative to the volume of the cavity. The solvent has low penetration capacity, therefore a cavity completely filled with resin is difficult to flush. If relatively more air is present in the cavity, flushing with solvent is more effective.

To summarize, cavities have to be flushed with solvent, which therefore should not be completely filled with resin after printing. The obtained parameters are listed in [Table 4](#). Channels with a diameter of 2.5 mm and larger can be printed and easily flushed. Hollow structures with a height of 20 mm allow for easy flushing. Walls with a thickness of 1.5 mm are robustly printable walls. If the wall thickness decreases further, we observed fast tearing of the walls.

Table 4: Obtained dimensional print limitations for printing pneumatic soft grippers with Elastic 50A.

Parameter	Value
Channel diameter	≥ 2.5 mm
Height of hollow structures	≥ 30 mm
Wall thickness	≥ 1.5 mm

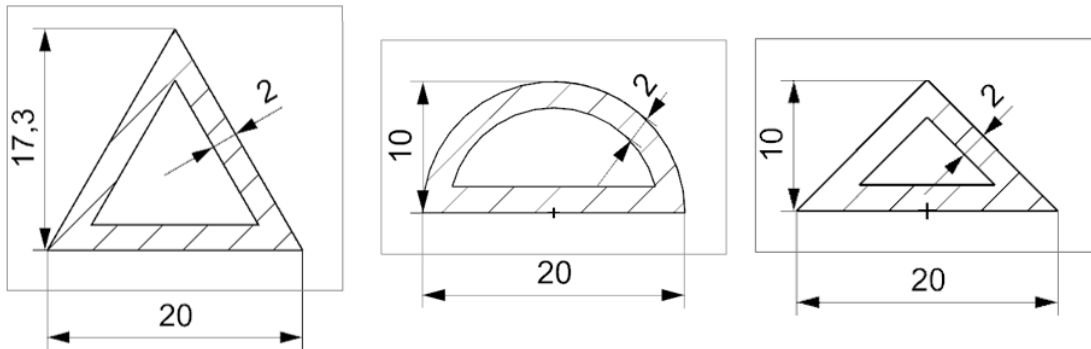


Figure 23: Three printed hollow shapes, at the bottom the dimensions of the model in millimeters. Top image depicts the half of the printed objects, while still having the supporting print structure at the bottom.

4.2 Material properties

In this section, the measurement results of the tensile tests will be presented and analyzed. As presented in [Section 3](#), we are interested in the following properties: Young's modulus, tangent modulus, hysteresis, and ultimate elongation. The Young's modulus is defined as the tangent modulus of the stress-strain curve at the initial strain. Strain can be defined as true strain and as engineering strain. Engineering strain is a linear approximation of true strain which holds for the low elongation regime. We measure at the large strain regime therefore true strain is a representation of the actual material behavior.

Specimen compensation

In [Section 3](#) we discussed the necessity of a geometrical compensation for the dogbone specimen. The compensation is calculated as described in Equations [2](#)-[4](#), which results in a compensation ratio of 1.0556[-]. This ratio is validated by a test measurement of six samples, of which three samples are a straight bar specimen and the other three are dogbone specimens. The measurement result is depicted in [Figure 24](#) in a tangent modulus plot. A tangent plot presents the slope of a stress-strain curve for the full range of measured strain values. In [Figure 24a](#) the data are depicted without compensation and in [Figure 24b](#) the data are depicted with the compensation applied to the dogbone specimens. We observe that in a) the bar specimens generally appear to have a lower tangent modulus compared to the dogbone specimens. This is in line with the defined hypothesis, expecting dogbone specimens to show a higher stiffness compared to the stiffness of bar specimens. In b) the compensation of 1.0556[-] is applied to the engineering strain of the dogbones specimens, prior to converting to true strain. In [Figure 24b](#) we observe no clear distinction between the tangent moduli of both specimen shapes, and therefore conclude that the compensation affects the data as expected.

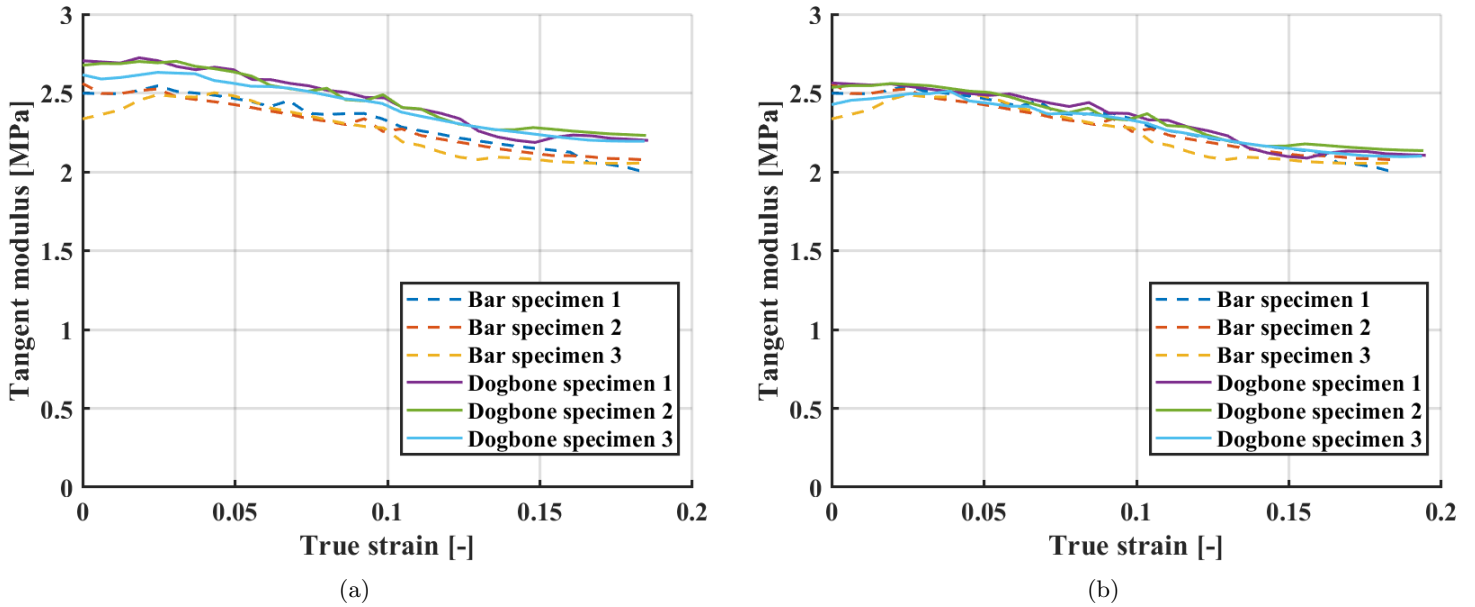


Figure 24: Tangent modulus curves with and without geometry compensation, for three bar shaped specimens and three dogbone specimens. a) No compensation has been applied, dogbone specimens appear to have higher stiffness compared to bar specimens. b) After compensation, the data show no clear distinction in terms of stiffness.

Specimen thickness

To convert the measured force data to stress, the thickness and width of the sample need to be measured. The specimens are printed horizontally on supports as depicted in [Figure 25](#), in which a) shows the specimen including the supports as visualized by the printing software and b) shows the print result after detaching the supports from the sample. We observe that the printer has difficulty printing the first layer on top of the supports, since this layer appears uneven. This layer lacks support between the supporting struts, which causes the resin to sag. This results in a specimen with an uneven bottom and therefore a non-uniform thickness.

The thickness has been measured using a thickness gauge that measures up to a hundredth of a millimeter. Each sample is measured on approximately 15 points, which are manually distributed over the entire surface. These data are presented in [Table 9](#) in [Appendix A](#). For each specimen the mean of the measured thicknesses of this single specimen is used for converting the force to stress.

Hysteresis

We are interested in the material behavior in terms of elastic hysteresis. Hysteresis is expressed as a percentage of the difference of y-values between loading and unloading, relative to the y-range of the cycle. Hysteresis is determined as explained for each cycle, namely for 5%, 10%, and 20% engineering strain. Using [Equation 1](#), hysteresis is calculated for each specimen, and subsequently the mean and 95% confidence interval of this mean are calculated. The data for each individual specimen are visualized in [Table 10](#) in [Appendix A](#). The summary of the data is presented in [Table 5](#).

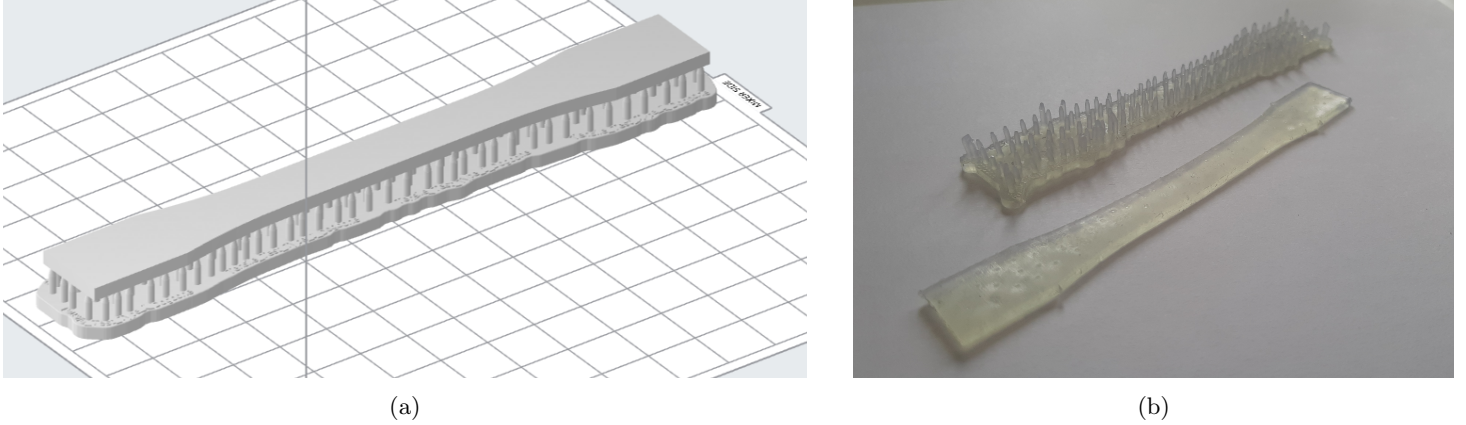


Figure 25: a) The dogbone specimen as depicted in the printer software, observed along with print supports. b) The printed dogbone specimen, below the detached print supports. It can be observed that the surface of the specimen is not flat but uneven.

We conclude from the data that the hysteresis percentage as well as the error are lower for larger strains compared to small strains. This inverse relation is caused by the definition of the hysteresis percentage which is calculated by dividing the difference of the load an unload cycle by the length of the strain range. The hysteresis of the material is of order size of a few %, from which can be concluded that hysteresis does not significantly impact the functionality of the gripper made from this material at the measured strain rate.

More detailed information on material behavior, for instance strain rate dependency, could have been investigated for hysteresis. Hysteresis in polymers is caused by viscoelastic material behavior, where damping and therefore hysteresis is dependent on strain rate. As shown, the hysteresis at the tested strain rate of $20\text{mm}/\text{min}$ are insignificant and therefore this strain rate dependency is out of the scope of this project.

Table 5: Results of hysteresis measurements. The data set consists of 15 samples. Each cycle is separated manually from the raw data of the cyclic measurements.

Cycle	Mean	95% CI
5 % ϵ_{eng}	3.146%	$\pm 1.065\%$
10 % ϵ_{eng}	2.079%	$\pm 0.588\%$
20 % ϵ_{eng}	1.065%	$\pm 0.364\%$

Elasticity

The Young's modulus is calculated for each specimen. Subsequently, these are averaged and we conclude that Young's modulus is equal to 2.63 ± 0.14 MPa. Afterwards, the data for each individual specimen are interpolated such that the data can be averaged. This average of the stress-strain curve for the 20% engineering strain cycle is presented in [Figure 26](#). In order to average the data, interpolation has been applied. To obtain an accurate average, the interpolation starts at 1% true strain. This eliminates the unreliable low strain data points, since not every data set obtains data below 1%. The curves of [Figure 26](#) are depicted also in [Figure 28](#) along with the 95% confidence interval error bar.

The elastic behavior is also depicted in [Figure 27](#) showing the tangent modulus as calculated from the loading curve of [Figure 26](#). At higher strains the tangent modulus decreases to approximately 2.2 MPa. A decrease in stiffness is generally caused by plastic deformation, but since the unloading curve shows this same shape in the stress-strain curve we expect that this does not hold. This behavior is therefore caused by non-linear effects. For instance, the alignment of the polymer chains in the strain direction in the high strain regime may be the cause of this behavior rather than plastic deformation.

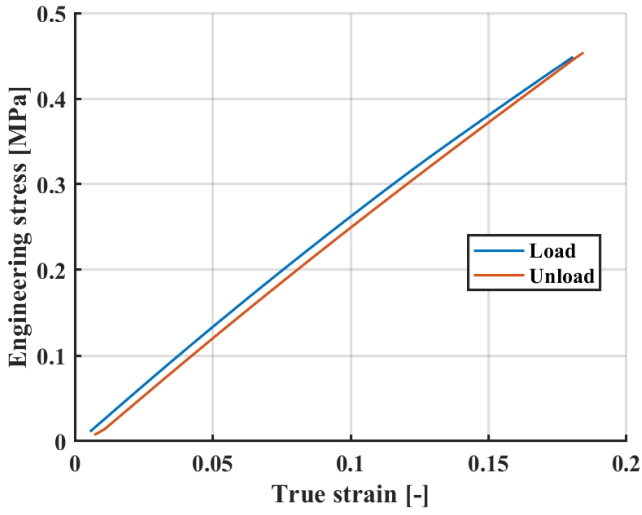


Figure 26: Stress-strain curve of the 20% engineering strain cycle. Loading and unloading data are visualized individually. This data is obtained from 15 measured specimens. The related errors are shown in [Figure 28](#).

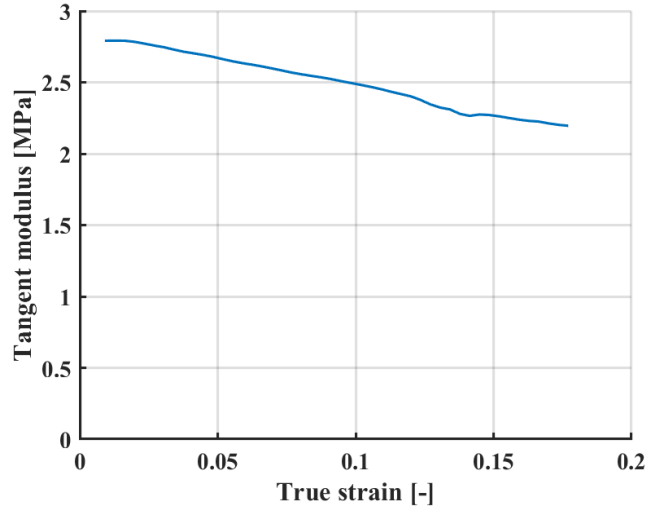


Figure 27: Tangent modulus obtained from the loading curve as depicted in [Figure 26](#), defined as the slope of the stress-strain curve.

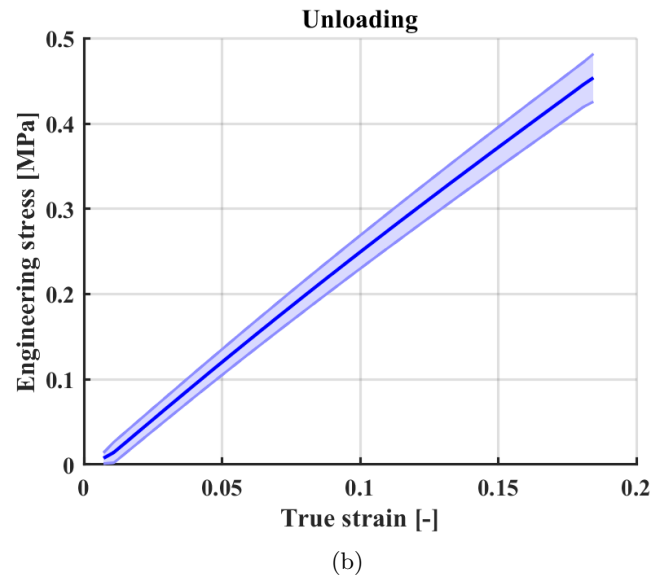
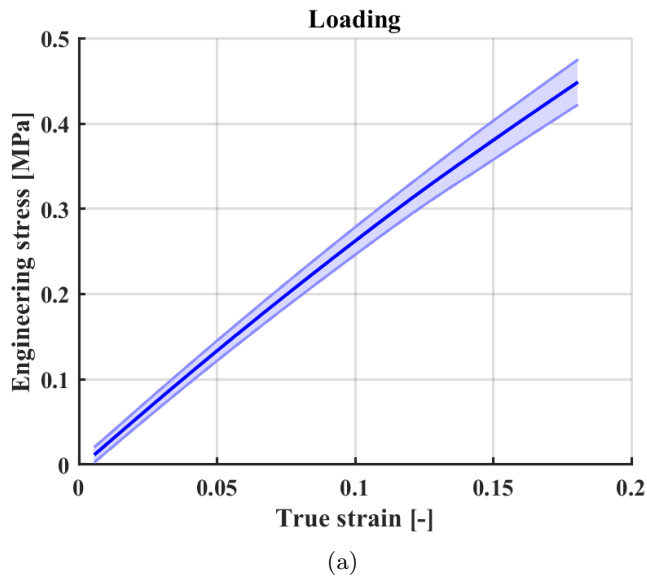


Figure 28: Stress-strain curve data for a) loading and b) unloading, along with the 95% confidence interval error bars, data obtained from 15 specimens.

Ultimate elongation

The ultimate elongation is determined as described in [Section 3](#). The individual data points at break for each specimen are depicted in [Figure 29](#). The corresponding stress and strain at break are shown in [Table 11](#) in [Appendix A](#), as well as the obtained stress-strain curves for the 24 specimens.

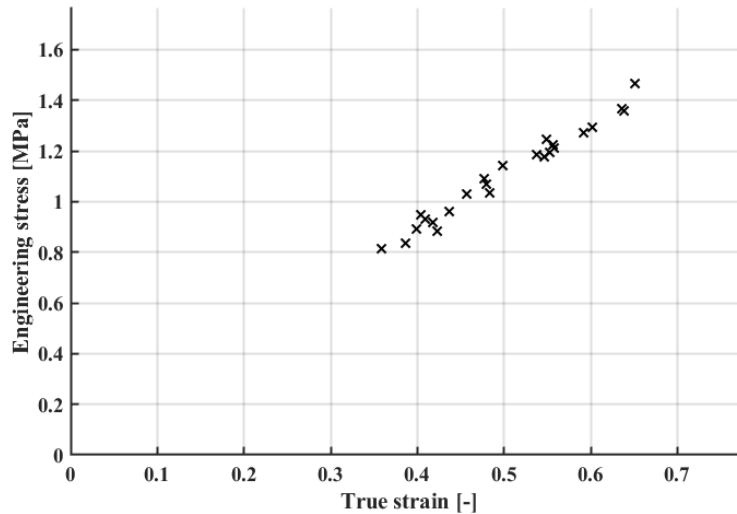


Figure 29: Stress-strain figure of ultimate elongation measurement. Data points indicate the point of break of individual specimens.

The fitted Weibull parameters with the 95% CI are:

- $\eta = 0.528 \pm 0.189$
- $\beta = 2.528 \pm 1.830$
- $\gamma = 0.305$.

The histogram of the ultimate true strain data as well as the Weibull probability distribution function is depicted in [Figure 30](#). We can conclude that the characteristic ultimate elongation is $\epsilon_{true} = 0.528 \pm 0.189$ and the failure free ultimate elongation is $\epsilon_{true} = 0.305$. The ultimate elongation is 160% as presented by Formlabs, which is equal to $\epsilon_{true} = 0.955$, as depicted in [Table 2](#). The presented values by the manufacturer are unrealistically high and not practically applicable.

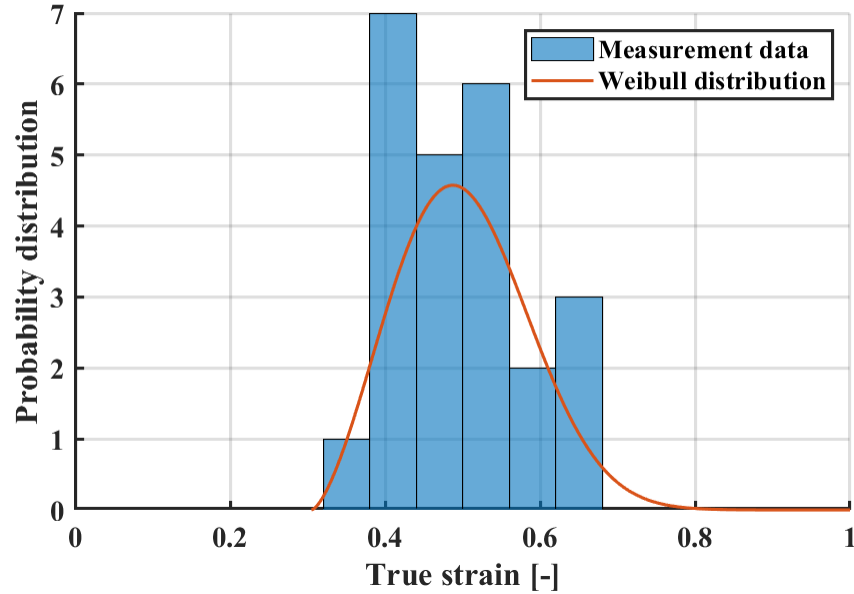


Figure 30: Histogram of the ultimate strain measured using 24 specimens. 3-parameter Weibull distribution probability function where, $\eta = 0.528 \pm 0.189$, $\beta = 2.528 \pm 1.830$ and $\gamma = 0.3050$.

Conclusion

To summarize the presented results of the material properties, we conclude that the Young's modulus is 2.63 ± 0.14 MPa whereas the tangent modulus decreases to 2.2 MPa in the large strain regime. Hysteresis is of the order size of a few % and therefore considered insignificant to the function of the gripper. The ultimate elongation calculations lead to a failure free ultimate elongation of $\epsilon_{true} = 0.305$ and a characteristic ultimate elongation of $\epsilon_{true} = 0.528$. These values are listed to compare to the values reported by Formlabs in [Table 6](#). It can be observed that Formlabs reported very large values for the material properties compared to what we measured.

Table 6: Measured material parameters compared to the parameters reported by Formlabs. [\[29\]](#).

Parameter	Reported value	Measured value
Shore hardness	50A	-
Young's modulus	-	2.64 ± 0.14 MPa
Ultimate elongation	$\epsilon_{eng} = 160\%$; $\epsilon_{true} = 0.955$	$\epsilon_{true} = 0.528$
Tensile strength	3.2 MPa	1.11 ± 0.37 MPa
Tear strength	19.1 kN/m	-

4.3 Soft grippers

As presented in [Section 3](#) in [Figure 15](#), two gripper designs are considered. Both designs have been tested initially and one design performed superior to the other. The straight design was pressurized and as a result, the observed bending deformation was approximately 45° when it ruptured at 2 bar. The balloon gripper was able to deform approximately 45° at a pressure below 0.5 bar and no rupture was observed up to 1 bar. This difference is due to the local deformation in the gripper. The straight design has to deform with in-plane bending of the sides, which requires high forces. For the balloon design, the only part that counteracts the bending is the bottom where the channels are located. Based on this fundamental test it can be concluded that the balloon gripper is more promising having higher force and deformation dependency on actuation pressure. Consequently, the straight design is rejected and the balloon design is further investigated.

The initial prototype of the single balloon gripper as presented in [Figure 16](#) lacked rigidity at certain sections. The final design is depicted in [Figure 31](#) which shows three improvements.

Firstly multiple edge blends have been added, such that the attaching surface from the balloons to the bottom is increased. This is necessary since the balloons function under large strains and therefore rupture is expected at this attaching surface.

Secondly, the first and last wall thicknesses are increased. The balloons provide the gripper with bending force by pressing onto each other and therefore bend the gripper. Since the first and the last wall have no adjacent balloon to press onto, the strain in this section will be the largest and it therefore is expected to rupture first. In addition, there is no functionality for this wall since it cannot create bending moment independently. Therefore, this wall is widened with respect to the rest of the walls by four millimeters.

Lastly, to enhance the forces that can be transferred from the gripper onto an object, the attachment from the balloons to the clamped section has to be stiff. Therefore this section is thickened and a chamfer is added onto the stiff side of the first balloon. The dimensions of the stated changes are indicated in [Figure 31](#).

During the project, multiple pneumatic attachment designs are tested. Since this is dependent on what type of pneumatic system will be attached and has no influence on the function of the gripper, this will not be presented in this report.

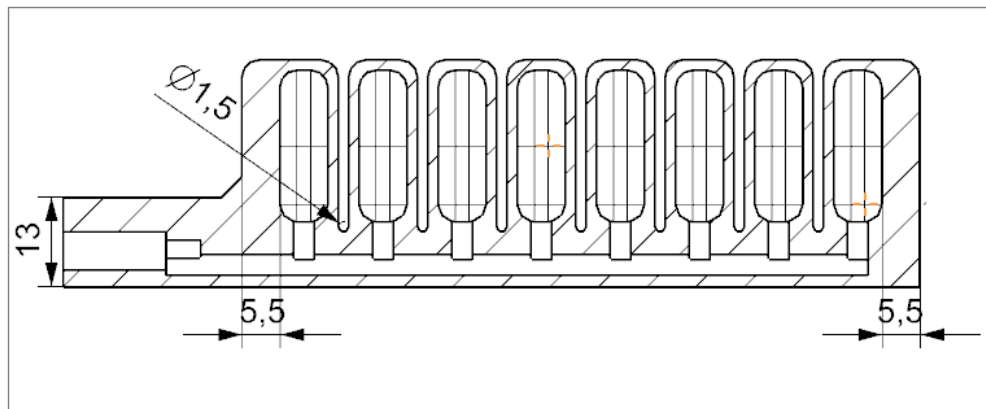


Figure 31: Schematic section view of the reference gripper, along with the dimensions of the improvements that are made compared to the initial prototype. Dimensions are presented in millimeters.

Force measurement

This section presents measurement results of multiple grippers. These grippers are printed with one single parameter modified from the reference gripper design in order to conclude directly how the single parameters influence the behavior of the gripper. The behavior of the gripper based on deformation, force, and their relation will be discussed in this section.

On the following pages, figures are presented side by side. On the left, figures a) represent the first height. This is where the tip of the gripper starts 30 mm above the load cell. On the right, in the figures b) this height is 44 mm. Firstly the two reference grippers are presented in [Figure 32](#) and [33](#). Consequently the effects of balloon height, wall thickness and bottom thickness are presented.

In [Figure 32](#) and [33](#) the force measurement results for the reference gripper are shown. First, the difference between the two measurement heights is observed as a shift of the data. Since the data appear linear, the shift can be considered a pressure and/or a force shift.

Since both grippers show comparable measurement data, we conclude that the printing process is repeatable. The pressure at which the gripper starts to touch the load cell, as well as the slope of the graph show similar values between [Figure 32](#) and [33](#).

For both grippers and both heights, measurement 1 shows deviating results compared to measurement 2 and 3. Initially, the measurement was executed, where only one data set was obtained for each reference gripper, measurement 1. After two weeks, the force measurement set-up has been rebuilt and data sets 2 and 3 were obtained. The shift in data may be caused by two factors: the installation of the measurement set-up and aging of the gripper due to exposure to sunlight for two weeks. As the set-up of the measurement is straightforward and no calibration has to be executed, the shift in the observed behavior is expected to be caused by additional curing or aging of the material.

The manufacturer does not provide any information about the curing process and whether the material is fully cured after the recommended post-processing. The material after post-curing shows undesired adhesion, which can be caused by unsaturated polymer chains, which indicates lack of full curing. When the material continues curing or aging, it is expected that the material shows an increase in stiffness since the number of crosslinks increases. The increase in stiffness is observed in both figures, since measurement 1 shows a lower dF/dP , compared to measurements 2 and 3. Therefore we assume that additional curing of the gripper caused this difference. We find that additional curing or aging is an important topic for future research. It is interesting to have insights in the lifetime of a gripper made from Elastic 50A and behavior changes over time depending on storage environment.

We observe hysteresis in the force measurements, since the unloading data points are different from the loading data points. As we stated in [Section 3](#), during measurements the gripper showed friction effects, which are located between the gripper and the load cell. This friction along with internal strain hysteresis of the material may cause hysteresis in the measurement data. The deformation measurement data that will be presented in [Figure 40-44](#) shows no hysteresis. Therefore the hysteresis in the force measurement is not caused by internal material strain hysteresis. Since the sliding constraint has low friction at low forces, the hysteresis of the measurement data is in line with the expectations of the friction effects. Therefore it is concluded that the hysteresis in the force measurement data is caused by the friction between the gripper and the load cell.

We will analyze the design parameters balloon height, wall thickness, and bottom thickness, by comparing the behavior to the reference gripper. We will focus on a shift and the dF/dP slope of the data. The definition of dF/dP is the force exerted per pressure increase. A higher dF/dP is a functional improvement. The dF/dP is quantified and depicted in the scatter figures on the next pages. A shift in the graph of the force measurement is primarily due to deformation behavior, which is discussed later.

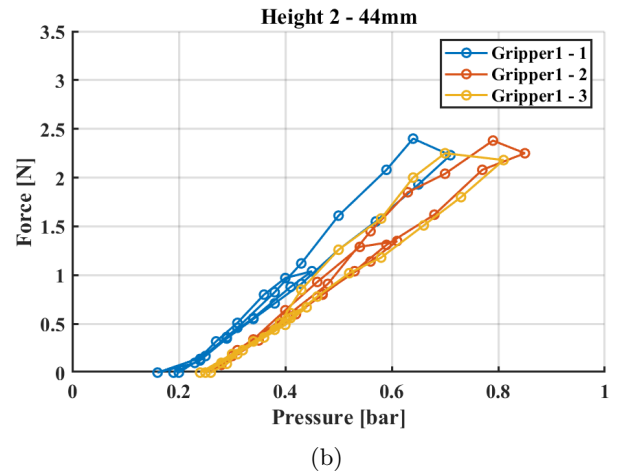
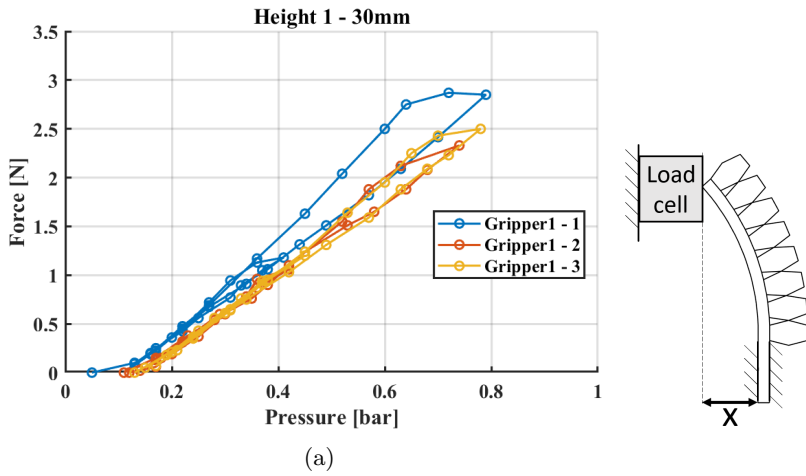


Figure 32: Force exerted by the first reference gripper dependent on actuation pressure. The same gripper is used for measurement three times, where measurement 2 and 3 are measured two weeks after measurement 1. Data are obtained at a height of a) 30 mm and b) 44 mm, which is indicated by x in the schematic image.

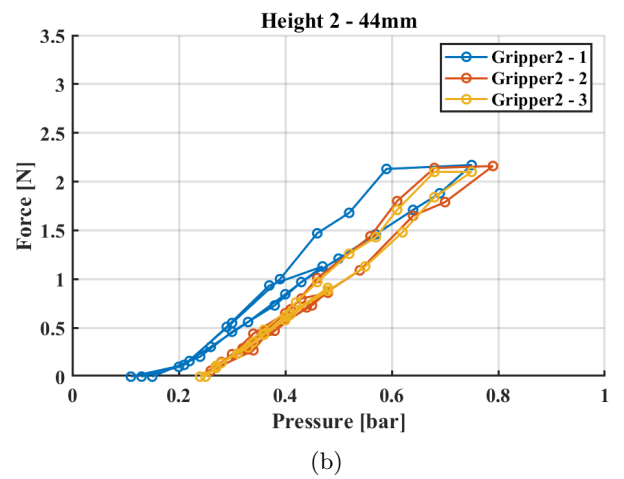
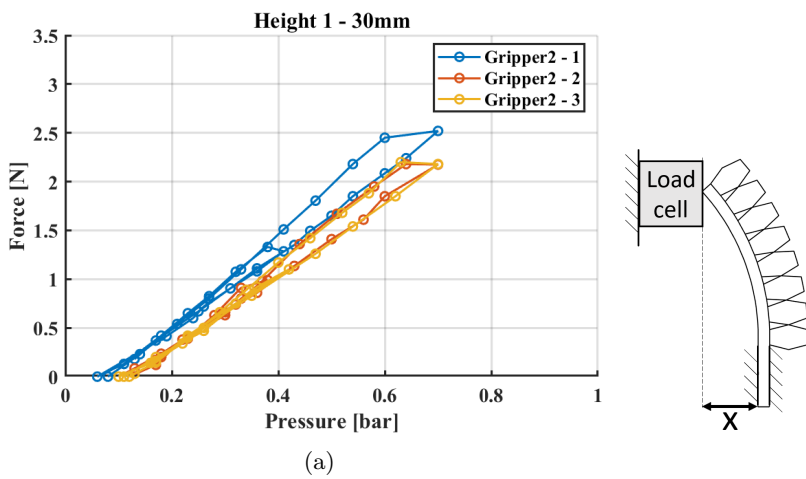


Figure 33: Force exerted by the second reference gripper dependent on actuation pressure. The same gripper is used for measurement three times, where measurement 2 and 3 are measured two weeks after measurement 1. Data are obtained at a height of a) 30 mm and b) 44 mm, which is indicated by x in the schematic image.

Balloon height

When analyzing the measurement results in [Figure 34](#) and [35](#), we observe a difference in dF/dP . The larger the balloon height, the higher dF/dP . The formulated hypothesis is that increasing the balloon height increases the moment of force created. This moment created by the balloons is converted into bending and force exertion on the object. Therefore the result is in line with the hypothesis that increasing the balloon height positively affects dF/dP .

It is important to note that during the printing process a limited printing volume is available for the model. When increasing the balloon height, the remaining distance between the gripper fingers decreases. Therefore using large balloon heights results in a decrease of the size of the object that can be grabbed. However this problem can be solved by applying negative pressures to bend the gripper outwards. This has not been investigated yet and is therefore included in [Section 6](#)

Wall thickness

As we observe in [Figure 36](#) and [37](#), increasing the wall thickness results in a decrease of dF/dP , and a shift towards higher pressures. Both effects are undesired, as the goal is to increase the dF/dP and exert forces at low actuation pressures. The hypothesis is that increasing the wall thickness increases the actuation pressure, but also increases the force that can be exerted. This hypothesis is rejected based on the measurement results. This can be explained by the balloons that will expand less, and therefore create less contact surface between the balloons. The surface on which the pressure acts to create bending forces decreases, which decreases the force that can be exerted.

Bottom thickness

In [Figure 38](#) and [39](#) we observe a shift of the data to higher pressures for larger bottom thickness, but comparable values for dF/dP . Therefore the bottom thickness primarily influences the deformation behavior. However, the bottom thickness does not influence the amount of force exerted. This is in line with the expectations since the bottom thickness parameter has no influence on the balloons, which are responsible for the force generation.

From the depicted scatter plots, we observe that the starting distance between the grippers and the load cell influences the dF/dP . This non-linear behavior affects the exerted forces most significantly in case of increased balloon height, less significantly for increased bottom thickness, and not significantly for wall thickness. This non-linearity is caused by the magnitude of deformation, in particular the bending angle of the gripper, at the point where the gripper touches the load cell. The exact physical cause of the difference in dF/dP has not yet been analyzed.

To conclude the force measurements, we found that increasing the balloon height and decreasing the wall thickness increases dF/dP , while changing the bottom thickness does not influence dF/dP . Decreasing wall thickness is preferred over increased balloon height when large forces are desired, due to the limitation in printing volume as explained earlier. However, wall thickness has a minimal dimension for ensuring robust printing. Although the data show approximately linear relation between the force and the actuation pressure, non-linear behavior is observed when changing the starting distance between the gripper and the object. The significance of non-linear effects differ per modified parameter and is not explained yet.

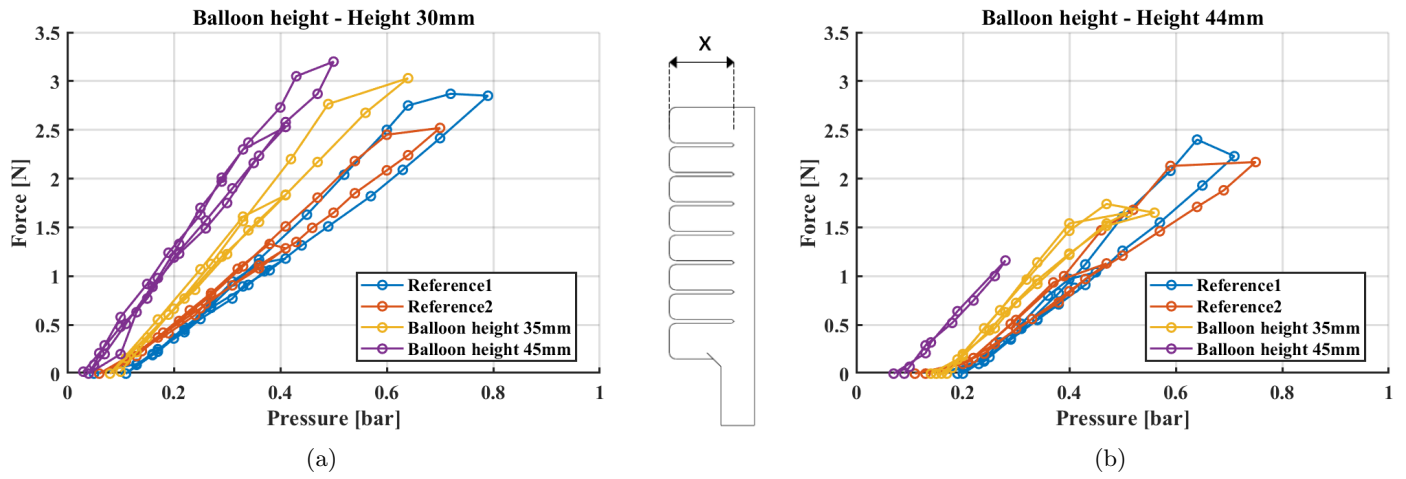


Figure 34: Force measurement result for changing balloon height, which is indicated by x in the schematic image. Data are compared to reference gripper 1 and 2 which have a balloon height of 25 mm. We observe that increasing balloon height results in a larger slope. Data are obtained at a height of a) 30 mm and b) 44 mm.

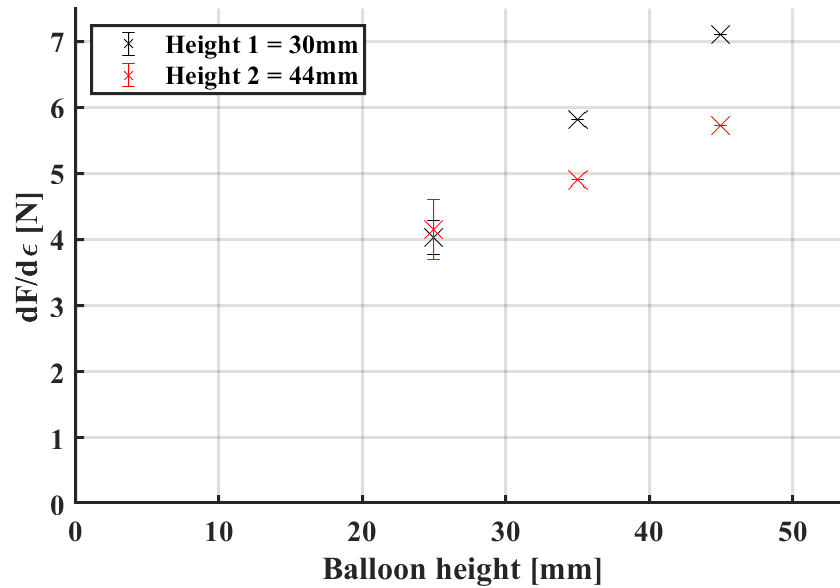


Figure 35: Slopes of linear approximation of force-deformation curves shown in [Figure 34](#) compared to the reference gripper measurements as shown in [Figure 32](#) and [33](#).

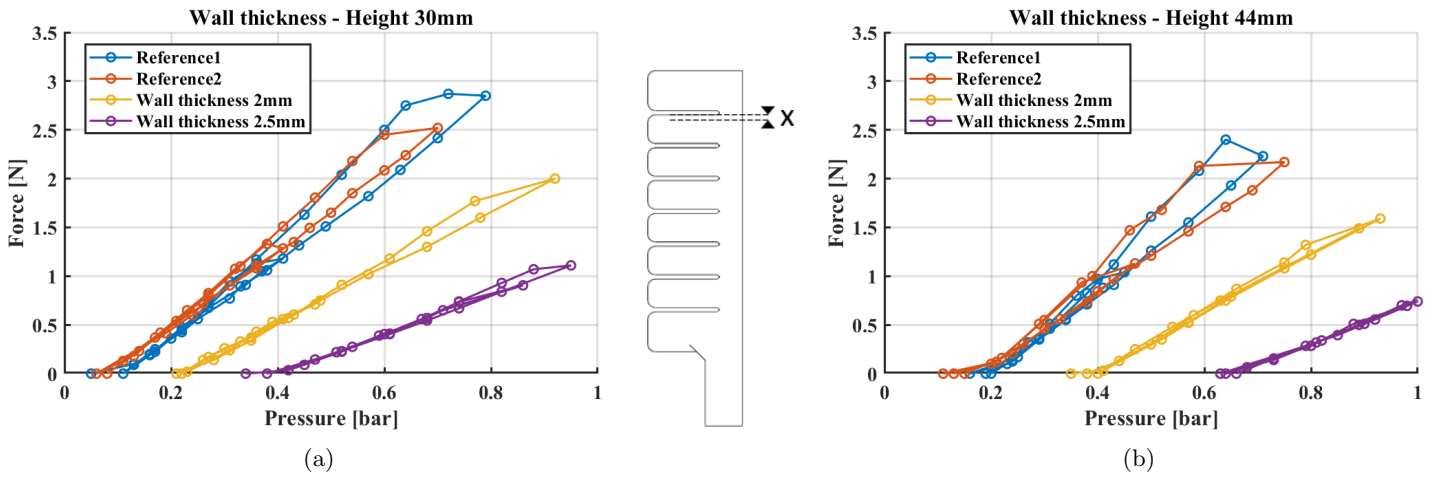


Figure 36: Force measurement results for increasing wall thickness, which is indicated by x in the schematic image. The wall thickness of reference gripper is 1.5 mm. The data show that increasing wall thickness has a negative effect, since the slope of the data is decreased. Data are obtained at a height of a) 30 mm and b) 44 mm.

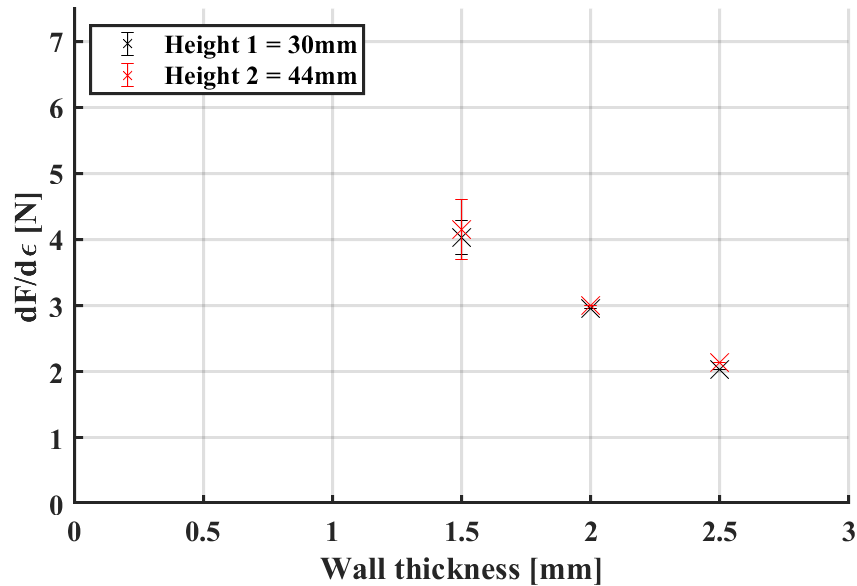


Figure 37: Slopes of linear approximation of force-deformation curves shown in [Figure 36](#) compared to the reference gripper measurements as shown in [Figure 32](#) and [33](#).

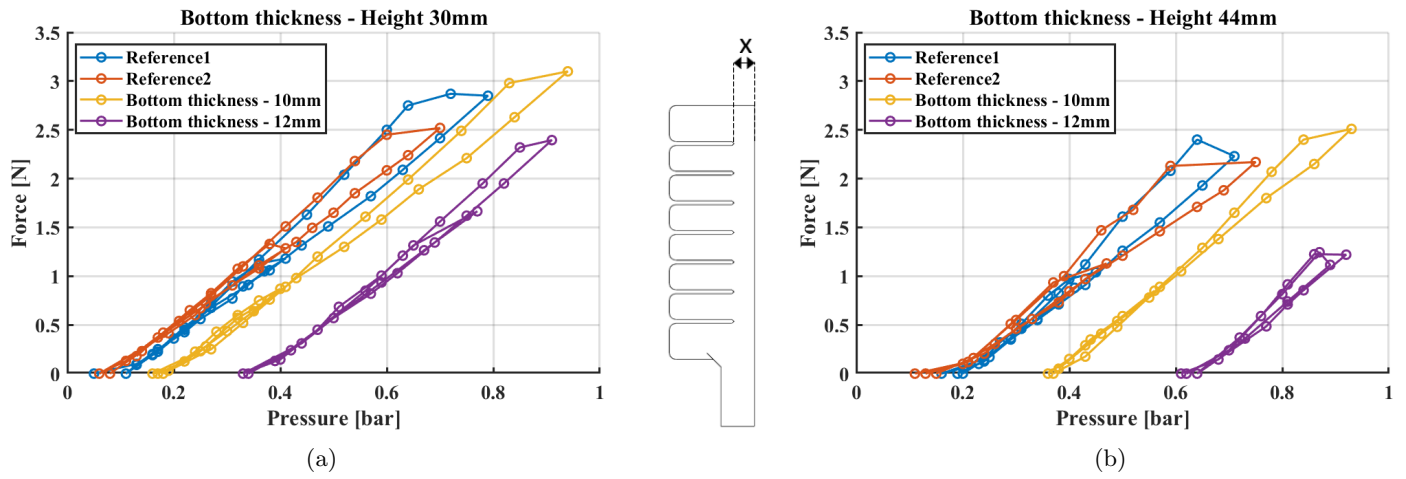


Figure 38: Force measurement results for increasing the bottom thickness, which is indicated by x in the schematic image. The data can be compared to the reference gripper which has a bottom thickness of 8 mm. The data show a shift, while having a comparable a slope. Data are obtained at a height of a) 30 mm and b) 44 mm.

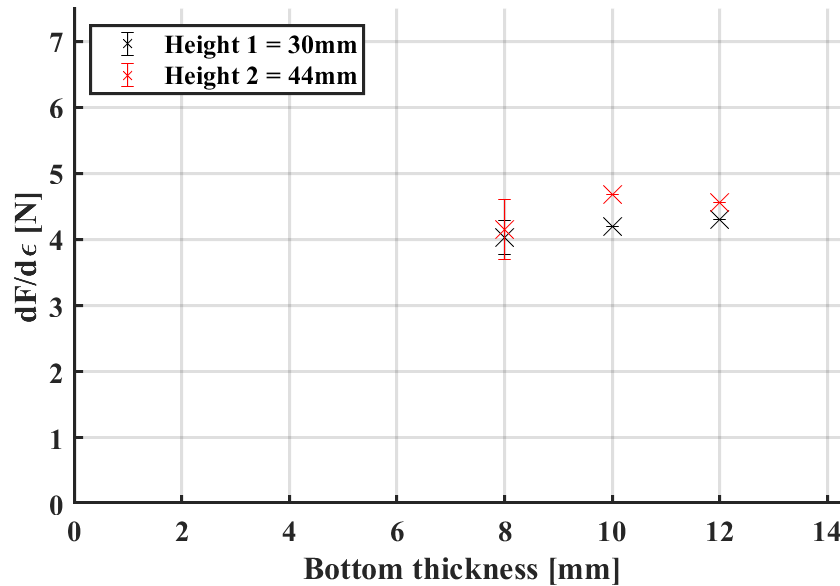


Figure 39: Slopes of linear approximation of force-deformation curves shown in [Figure 38](#) compared to the reference gripper measurements as shown in [Figure 32](#) and [33](#).

Deformation measurement

The deformation is quantified by the horizontal displacement of the tip which depends on the actuation pressure. The measurement set-up has been shown in [Figure 18](#). The quantification of the deformation can be used to predict the pressure at which the gripper touches an object. When picking relatively small objects, it is necessary to have large deformation at low pressures. If this is not the case the actuation pressure is close to the maximum of the operating range when touching the object. It is necessary to increase the pressure further to exert force on the object to obtain a firm grip. Therefore, depending on the application and the desired object size and mass, this deformation relation is an important design factor.

From the data in [Figure 40-44](#), we observe no hysteresis. This proves that the gripper has no significant internal hysteresis caused by the material, as this did not influence these particular measurements. Based on the absence of hysteresis in the deformation measurement data we confirm that the hysteresis in the force measurement is caused by the measurement method rather than by internal effects in the material.

Reference gripper

From both [Figure 40](#) and [41](#), we observe that the resulting data are approximately equal. It is important to note that in contrast to the reference force measurement, all measurements have been executed within a short time frame. Therefore differences due to undesired curing times do not affect this measurement.

Balloon height

In addition to the positive results for increasing the balloon height in the force measurement, the obtained data show larger deformation at the same pressures. This is in line with the expectation since larger moment of force of the balloons will create larger deformation.

Wall thickness

[Figure 43](#) shows that increasing the wall thickness decreases the deformation significantly. This is in accordance with the expectation since increasing wall thickness reduces the amount of deformation of the balloons, and therefore also the deformation of the gripper.

Bottom thickness

In the force measurement, the bottom thickness showed no clear influence on the slope. In contrast, it does influence the slope of the deformation curve as shown in [Figure 44](#). Increasing the bottom thickness will increase the resistance to bending, therefore a higher moment of force induced by the balloons is necessary to deform the gripper.

To conclude, the measured deformations are in line with the expectations. Since we focus on global functioning of these grippers, there are no specific conclusions that can be drawn. When this gripper will be developed for use in a particular application, the presented data can be used to gather information to link the operational requirements to design parameters. If one is interested in picking an object with an approximately known size with a desired clamping force, using the data from [Figure 40](#) to [44](#) can be used to predict at what pressure the gripper touches the object. The data from [Figure 32](#) to [38](#) can be analyzed to obtain the pressure at touch. Subsequently the pressure increase to reach the desired clamping force can be calculated. It is important to note that the pressure does not exceed the known safe operating pressure of roughly 1 bar.

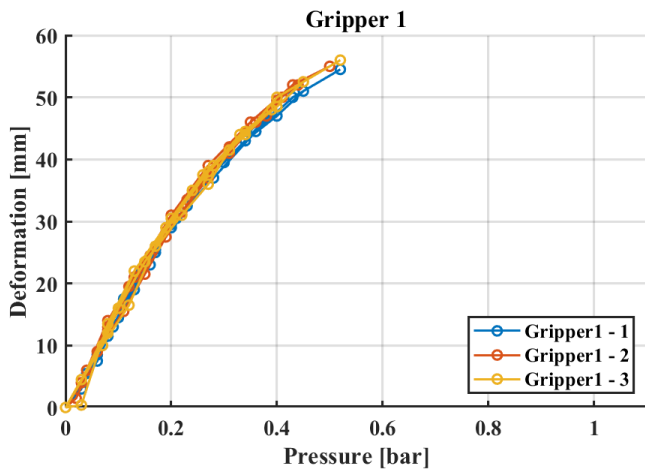


Figure 40: Deformation measurement of reference gripper 1. The measurement has been executed three times, validating repeatability of the measurement.

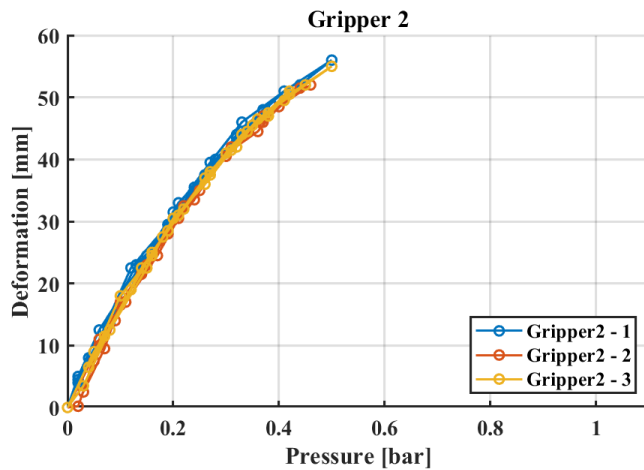


Figure 41: Deformation measurement of reference gripper 2. The measurement has been executed three times, validating repeatability of the measurement.

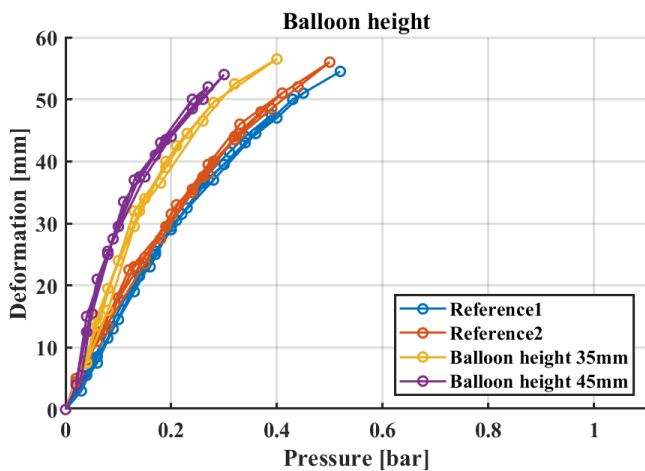


Figure 42: Deformation measurement results of increasing the balloon height. The reference balloon height is 25 mm. Increasing the balloon height shifts the deformation curve towards the lower pressure regime.

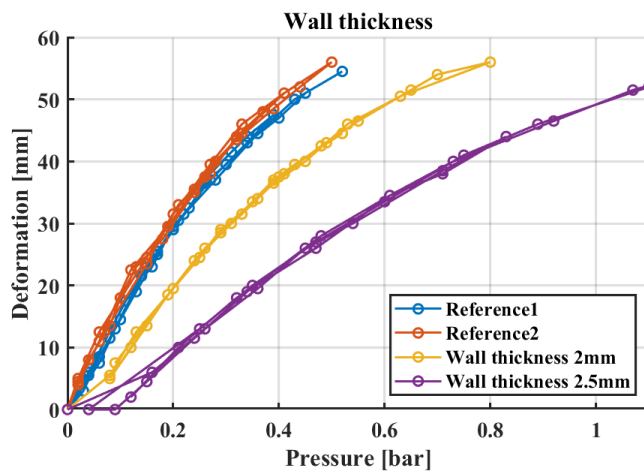


Figure 43: Deformation measurement results of increasing the wall thickness. The reference wall thickness is 1.5 mm. Increasing the wall thickness shifts the deformation curve towards the high pressure regime.

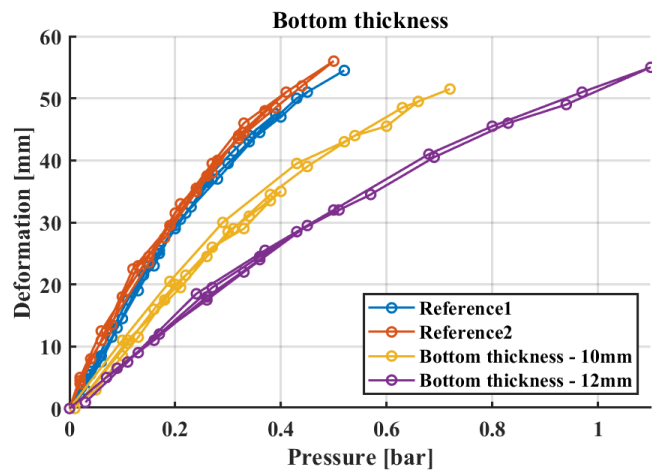


Figure 44: Deformation measurement results of increasing the bottom thickness. The reference bottom thickness is 8 mm. Increasing the bottom thickness shifts the deformation curve towards the lower pressure regime.

4.4 Gripping demonstration

During development of the gripper we focused on the ability to pick objects of different sizes, shapes, and masses. Therefore five everyday objects are used to demonstrate the grabbing ability of the gripper. The objects that have been tested by the developed gripper are listed in [Table 7](#)

Table 7: Five everyday objects that are used to demonstrate the picking ability of the soft gripper.

Object	Shape	Mass	Surface
Table tennis ball	Sphere	3 gr	Smooth plastic
Cube Elastic 50A	Cube	29 gr	Rubbery
Massage ball	Sphere	180 gr	Rubbery
Coke can 250mL	Cylindrical	272 gr	Smooth metal
Box of screws	Cuboid	583 gr	Smooth plastic

The gripping ability of the gripper is based on three principles: actuation, stiffness, and adhesion. Actuation is picking based on the force of the gripper exerted on the object. The stiffness principle is based on the soft property of the gripper which allows the gripper to adjust its shape and therefore to lift an object. Adhesion is based on the friction between the object and the gripper. These principles are shown in [Figure 45](#), presented by Shintake et. al. (2018) [\[1\]](#). The gripping ability of a soft gripper is shown for each combination of gripping principle and object shape. It is observed that for each gripping principle different shapes show varying difficulty of gripping.

During the demonstration of the objects presented in [Table 7](#), we observed that each object has its own gripping difficulty. A video of the demonstration can be found by following the QR-code on the next page. Snapshots of the video are depicted in [Figure 46](#), they show that the gripper is capable of picking each tested object. We will further discuss the picking ability per object in the remainder of this section. [Figure 45](#) will be used to analyze the observed results.

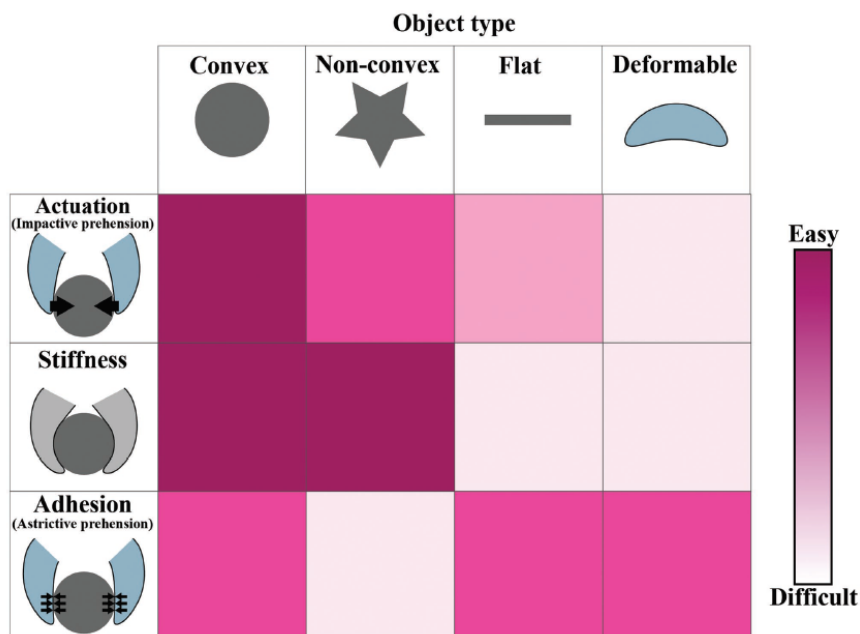


Figure 45: Soft gripper difficulty for four shapes and three gripping principles. [\[1\]](#)

Table tennis ball

The table tennis ball has a mass of 3 grams and has a spherical shape with a small diameter. We observed that the gripper was able to create a firm hold on the ball with fairly low pressures. The hold is based on a combination of the three factors: actuation, stiffness, and adhesion. Neither one of them is observed as the primary factor. The actuation is able to push firmly on the ball. The stiffness of the gripper allows to grab under the ball to increase the grip. The adhesion is moderately improving the grip. The combination of these factors in addition to the low forces by gravity and acceleration create a firm grip for the gripper on the table tennis ball.



QR-code to the video of the demonstration. Video also available at youtu.be/8cIlewpZ0g8.

Cube of Elastic 50A

This cube is made of the same material as the gripper and has a mass of 29 grams. We observed that the gripper can pick this cube firmly without having to exert high forces. This is caused by the high adhesion between the gripper and the cube. The adhesion is therefore the primary principle of gripping this cube. The stiffness of the gripper has no advantages regarding grabbing this cube, since it is observed that only the tip of the gripper makes contact and creates grip due to adhesion.

Massage ball

The massage ball is made from plastic/rubbery material and has a mass of 180 grams. We observe that the mass of the ball plays an important role when moving the gripper around while holding the ball. The gripper is not able to hold the ball firmly. Although the gripper shows fairly good adhesion to the ball, the gripper is not sufficiently wide to ensure stiffness based gripping in all directions. Adding a third finger to the gripper would significantly improve grabbing this spherical object.

Can of coke

The next object is a can of coke of 250mL, which has a mass of 272 grams. The object is cylindrical and the gripper has very low adhesion to the surface of the can. The gripper is able to pick up the can, but when the gripper is moved around it loses grip of the object. Due to the shape of the object, the stiffness property does not contribute to the grip. If the can slides through the gripper, the gripper regained its grip by hooking to the small protruding top edge of the can. Using this edge, the gripper created a firm grip on the can. Based on global properties of this object, the grip is insufficient for a firm grip. When using smaller features such as the top edge, the can could be grabbed firmly and move around without losing grip.

Box of screws

The last object is a box of screws that weighs 583 grams. We observed that the gripper is able to grab the box, while we limited the acceleration such that no other forces than gravity act on the object. The gripper does not benefit from its stiffness due to the flat surface of the object. In addition, the adhesion of the gripper to the box is low. Similar to the coke can, the box would slide through the gripper when acceleration forces are induced. Nevertheless, the grip is regained when the tips of the gripper are able to grab the small overhanging lid.

To conclude this demonstration, the gripping ability is dependent on multiple factors. Size and adhesion properties play an important role. In addition, small details in design of the object can increase the gripping significantly, as seen with the can of coke and the box of screws. It is demonstrated that the gripper is able to pick objects of multiple shapes and masses up to 583 grams. When the approximate shape or mass or any other object properties are known, one can adjust the dimensional parameters as well as the number of fingers on the gripper for specific application. Furthermore, when testing objects more specifically, one should know what order of acceleration can be expected in practice. During this demonstration the acceleration is the primary factor causing the gripper to lose grip of the objects.

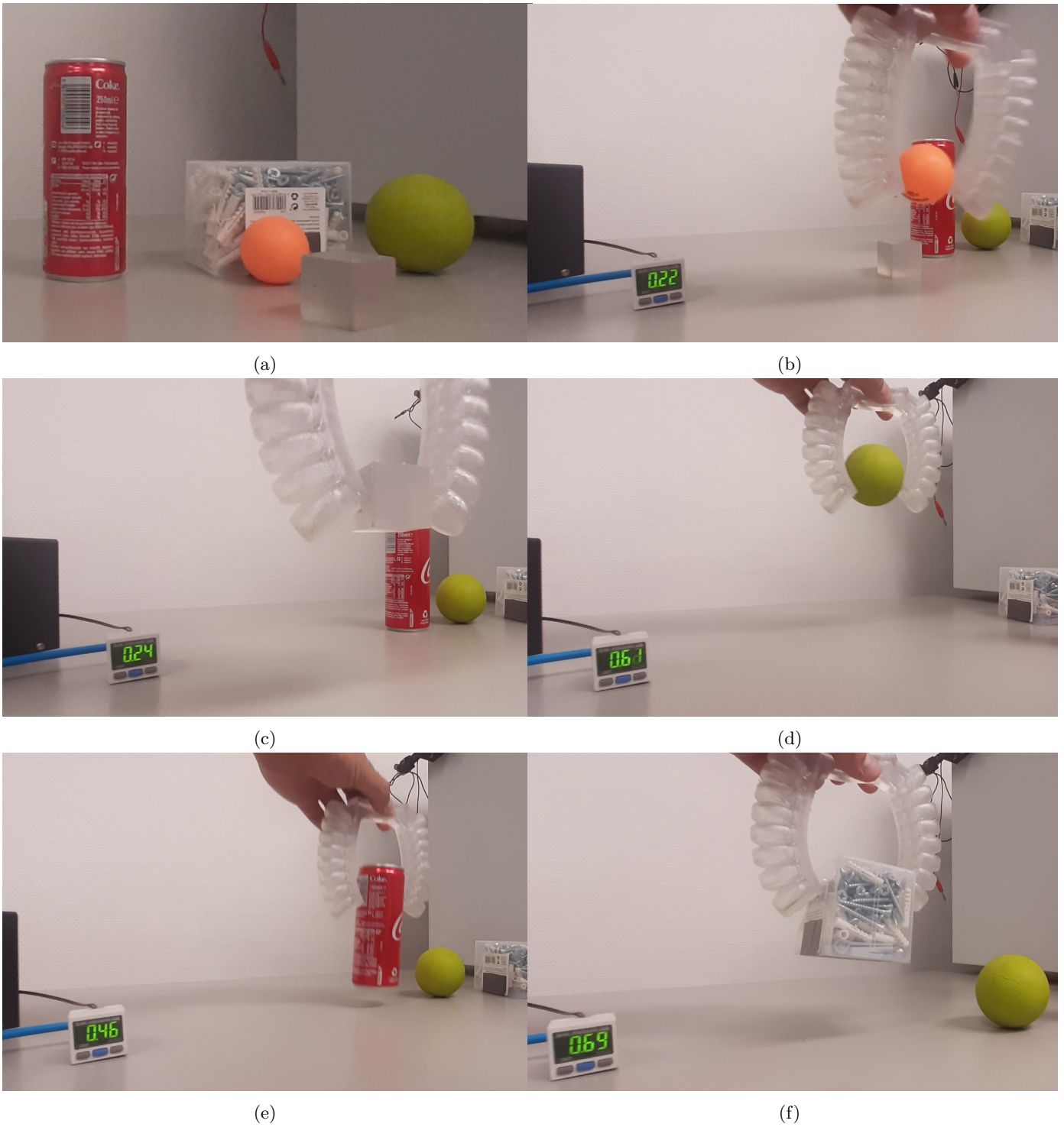


Figure 46: Video snapshots of picking demonstration. a) Image of the five objects. b) Table tennis ball of 3 grams. c) Cube of Elastic 50A material of 29 grams. d) Massage ball of 180 grams. e) Can of coke of 272 grams. f) Box of screws of 583 grams. Displayed number represents the actuation pressure in bar.

4.5 Valve

The purpose of the developed valve is to hold a pressure in a closed system that is attached to the valve. A functional requirement is that the valve does not leak through the valve-seat. If any leakage is present, the pressure that actuates the valve decreases which therefore increases the loss of air. The height and diameter of the valve are 55 mm and 50 mm, respectively. To be able to define elastic sections and stiff sections made from the same material, one is bound to make certain sections thick compared to others.

In [Figure 21](#) the initial prototype for the valve has been shown. The valve which is printed at an angle on the build platform, along with the printing supports are depicted in [Figure 47](#). Internally no supports can be present, since it is not possible to remove them after printing. The valve should be printed at an angle since each layer has to be partially in contact with the previous layer for stability purposes during printing. Even when printing at an angle, the print is not stable at each printed layer. As depicted in [Figure 47b](#), the software shows a red area that indicates a lack of support. It is important to note that during the design process the valve stem is critical for the printing process, but despite the warning of the software the valve can be printed properly in the shown orientation.

When testing this prototype valve with pressurized air, we observed that the valve movement works as intended. This could not be captured since the material is opaque. However, we were able to observe the movement of the membrane. The membrane moves up when pressure is increased and it returns when pressure is released. The valve was not able to close off due to lack of sealing. At a certain point the valve stem got pulled through the valve seat due to deformation of the valve seat. This deformation is undesired and requires support. Although it is three times as thick as the membrane, the valve seat still shows significant deformation. When the valve seat deforms, the valve stem is unable to create a seal which is necessary to prevent air flow.

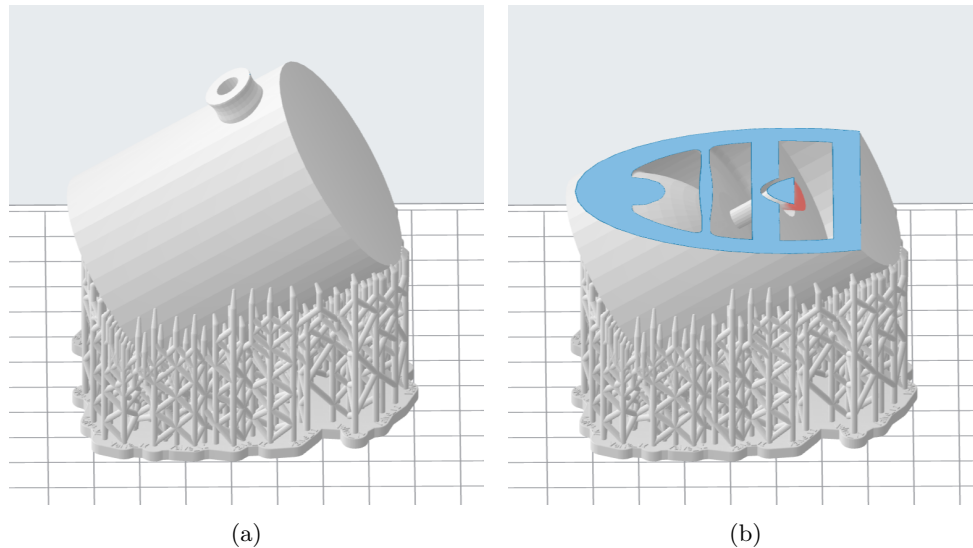


Figure 47: Initial valve design in Preform software provided by Formlabs. a) Shows the valve with the attached print supports. b) Shows the print-layer at the unsupported part of the valve. The red area is shown by the software to indicate where the part is in need of additional support for printing.

After printing and testing, the valve has been cut open to analyze the internal structure. This is shown in [Figure 48](#). The rough surfaces are due to the cutting process. It can be observed that the printing process is able to produce the valve properly since there are no defects visible. The design has to be adjusted such that the valve stem will be larger compared to the valve seat. In addition, the depth stop should be more stiff so it will not buckle. Furthermore, the deformation of the valve seat should be as small as possible to enhance sealing.

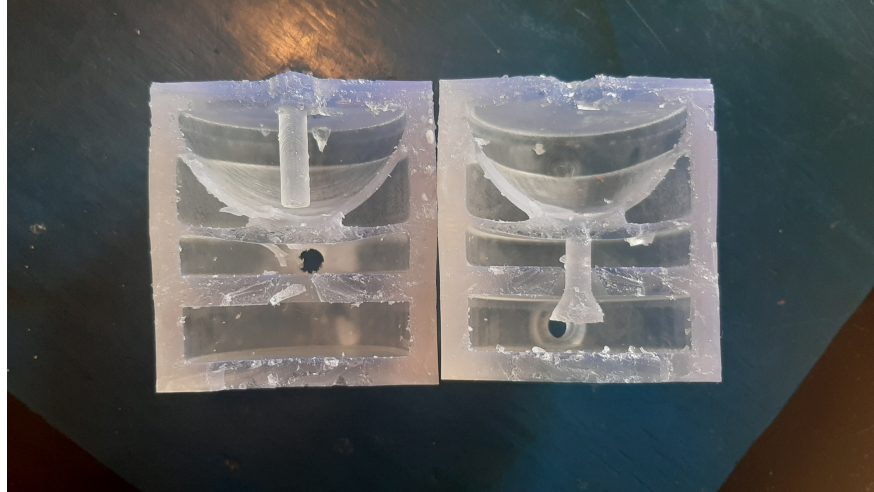


Figure 48: The printed initial valve which is cut open through the center. The printed surfaces are smooth, in contrast to the rough surfaces caused by the cutting process. Valve and depth stop appear to be flexible due to low dimensions.

In order to mitigate the risk of rupture and to improve the printing process, chamfers and edge blends have been applied to the final design of the valve. The valve should be as compact as possible, therefore the dimensions are decreased where possible.

Going through multiple prototyping steps, the final design is obtained. This design is shown in [Figure 49](#). a) Shows the section view of the valve, in which the design can be observed. The valve stem has increased in size compared to the valve seat. The deformation of the valve seat is opposed by pillars and the depth stop is more rigid. The relevant parameters are shown in [Figure 49](#)b. At initial testing this valve proved to be capable of sealing the air, and therefore functions as intended.

To gather information on the function of the valve, the following test has been executed. The actuation pressure regulator will be attached to the inlet of the valve and a closed arbitrary system will be attached to the outlet of the valve. The property of interest is whether or not the valve closes at certain pressures. Therefore, the pressure is increased and subsequently released. The pressure in the system is measured and validated whether it returns to ambient pressure or stays at the elevated pressure. The measurement result is shown in [Figure 50](#). The measurement points are indicated by an O or X, whereas the dashed lines indicate the sequence of the measurement points.

We observe that the system pressure increases along with the actuation pressure. In addition, when the actuation pressure is relieved, the system pressure is relieved as well. This is due to the fact that at the low pressure regime the valve is not fully closed. The behavior changes above a certain threshold. From the actuation pressure of 0.5 bar, the valve is able to close and therefore the system pressure is preserved. To continue the measurement, the system pressure is manually relieved to open the valve. For each data point larger than 0.5 bar, the same behavior is observed. At the pressure of 1 bar the bottom of the valve ruptured due to excessive strain.

The system pressure shows a pressure drop when the inlet pressure is relieved and the valve is closed. This is caused by the deformation of the valve due to the actuation pressure. It is observed that the valve shows extension in the radial direction of the valve along with the deformation of the valve seat. Both deformations are induced by actuation pressure and therefore these are returned to the original state when the actuation pressure is relieved. The valve returning to the non-deformed state causes the volume of the closed system to increase which consequently causes the pressure drop.

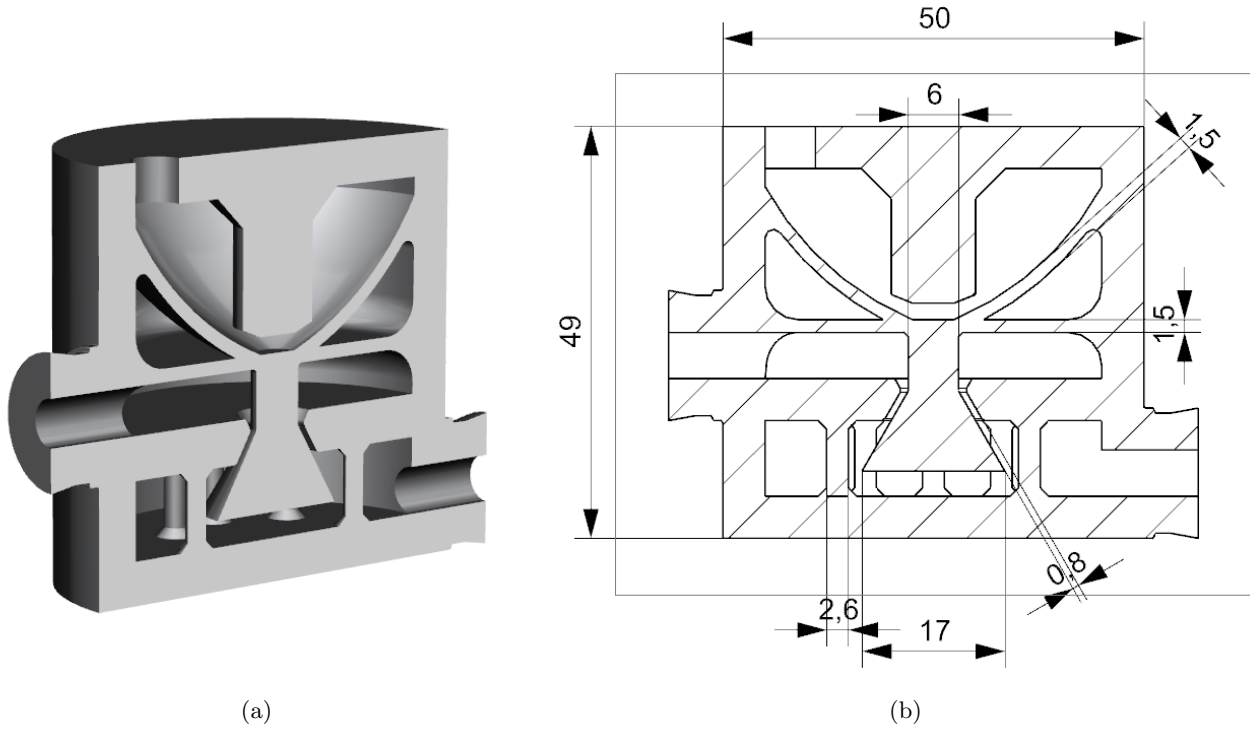


Figure 49: Section view of the final design of the valve. a) The image of the intersection of the circular design. b) The intersection of the valve with the spatial parameters of functional features.

For integration of the valve in a soft gripper, the dimensions of the valve are currently too large. The large dimensions of the valve are due to the limitations of the printing process. Since the used printing machinery has been on the market for a few years, we expect that print resolutions will be increased in the upcoming years. When the possibilities with respect to printing using these commercial machines increase, future research can be conducted whether or not integration in the proposed gripper is feasible.

It can be concluded that the valve shows functionality as expected and therefore this is a proof of concept supporting further development of this valve. The valve is monolithic, 3D-printed, and can hold pressures above a threshold pressure. For the current design the threshold is 0.5 bar. In combination with other types of valves this valve can provide a complex actuating system using a single tethered connection. The expected increasing print resolutions may give more opportunities for valves to be integrated in the future.

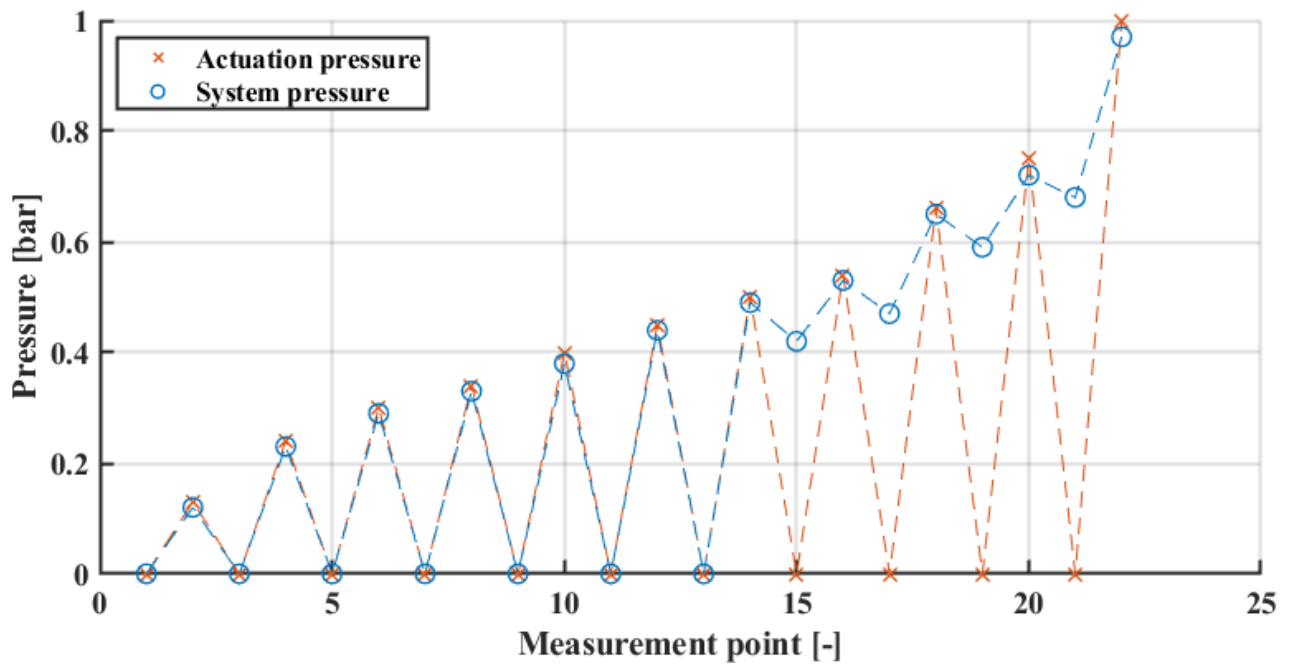


Figure 50: The measurement result of the valve. The actuation pressure is the inlet pressure applied to the valve. The system pressure is measured behind the valve in the attached closed system. Dashed lines indicate the measurement sequence. Data points indicated by an O or X are measured values. After measurement points 15, 17, 19, and 21, the system pressure is manually relieved to open the valve and to continue the measurement.

5 Conclusions

This research aimed to develop a multiple degree-of-freedom soft gripper with a single tethered connection. Based on qualitative and quantitative analyses of the developed gripper we conclude that a soft gripper has been developed and the functional effectiveness has been verified. However, the implementation for multiple degree-of-freedom actuation has to be developed further. Soft grippers are necessary in industries to pick delicate objects from which the dimensions are not exactly known. This research provides a soft gripper and an assessment of the impact of the design parameters on its functionality. By adjusting these design parameters the soft gripper can be adjusted with focus on a specific application. The soft gripper has been used for demonstration by picking up objects from 3 to 583 grams, with dimensions from 4 up to 8 centimeters including both spherical and cubical shapes.

The material properties are determined by a displacement controlled tensile tester. The Young’s modulus is determined to be $2.63 \pm 0.14 [MPa]$ from 15 specimens. The failure free ultimate elongation is $\epsilon_{true} = 0.305$ and the characteristic ultimate elongation is $\epsilon_{true} = 0.528 \pm 0.189$, determined by the Weibull distribution fit with 24 specimens. The hysteresis is determined to be of the order of a few % and decreases when operating in the large strain regime.

Using the Formlabs machinery and Elastic 50A material, the minimal print parameters are determined. Wall thickness of > 1.5 mm, hollow structure height of > 20 mm and channels of > 2.5 mm in diameter show good printable results. Multimaterial printing appeared not yet possible in the current production process. Additional research should be conducted to investigate whether functional, for example conductive, material can be implemented or added onto the printed gripper. The advantage of using 3D-printing over conventional casting and molding is primarily the design freedom. Using casting and molding, the design is constrained to a layered structure. However, by using 3D-printing the need for a layered structure is eliminated and the above stated three print parameters should be primarily taken into account. Therefore 3D-printing allows for more sophisticated designs, which allows for better actuation possibilities, such as presented by the soft gripper. In addition, multiple degree-of-freedom actuation is not yet possible using 3D-printing, but a proof of concept of a valve is shown which is not feasible to produce by casting and molding.

Design parameters of the soft gripper that influence the functionality are: wall thickness, balloon height, and bottom thickness. These parameters can be used to adjust the functionality of the gripper to a specific application. Increased balloon height and decreased wall thickness increases the actuation force exerted onto an object. The bottom thickness primarily influences the deformation behavior of the gripper. The gripper with an increased balloon height was able to exert the maximum force of 3.2 N at a pressure of 0.5 bar.

In addition to the soft gripper, this research has focused on the development of advanced actuation principles. This research presented a close-off valve as proof of concept for further development. This valve is 3D-printed from the same material as the soft gripper. The valve is normally opened and can be actuated by the main fluid flow. The valve can keep a system pressurized above a threshold while releasing the inlet pressure. The threshold pressure for the presented design is 0.5 bar. Integration of this valve is not yet possible due to limitations of the printing process. The valve is in the same order of size as the soft gripper, while an order of dimension smaller is necessary for integration in the soft gripper. This valve shows proof of concept as a starting point for further development to create a full set of valves which allows for multiple degree-of-freedom actuation.

The presented soft gripper is in terms of functionality currently not superior to the commercially available gripper of Soft Robotics Inc. The specifications of the two grippers are compared in [Table 8](#). The presented specifications for the developed grippers depend on the design parameters which can be adjusted. The main advantage of the developed gripper over the gripper of Soft Robotics Inc. is the possibility regarding further implementation of complex internal structures. If research is conducted on decreasing the size of the presented monolithic valve, this can be implemented in the developed gripper. On the contrary, the commercial gripper shows no possibilities regarding increasing functionality other than adding spacers of the modular system.

Table 8: Performance of developed gripper compared to the commercially available gripper.

	Developed gripper	Soft Robotics Inc.
Operating pressure	0 up to 0.9 bar	-0.35 up to 0.7 bar
Maximum force	3.2 N	8 N
Stroke	>100 mm	100 mm
Further development opportunities	✓	x

To conclude, a functional gripper has been developed, presented and analyzed. Functional dependency on design parameters is known and can be used for design for specific application. A proof of concept valve has been developed and can further be investigated for the ability to be integrated in functional systems. Recommendations for further research are presented in the next section.

6 Future research

6.1 Soft gripper design

Although the primary design parameters that influence the function of the gripper have been analyzed, three parameters still have to be investigated, namely the width and length of the gripper, and the number of balloons. To elaborate, increasing the width of the gripper can influence the gripper behavior. We expect that by increasing the width, the actuation creates a higher bending moment, whereas a wider bottom counteracts this bending. The specific relations of the bending moments and forces are still unknown so it is interesting to investigate this parameter.

In operational testing an important parameter which has not been investigated is the span of the gripper. The reference span for the gripper has been measured as the zero-pressure distance between the finger tips, rather than bending the fingers outwards. We expect that applying negative pressure to the gripper causes the balloons to contract, and therefore causing the gripper to bend open. This increases the span of the gripper without the need to use a larger print volume.

Performance of the gripper can possibly be enhanced by tuning the adhesion property of the gripper. This may be achieved by investigating chemical and physical properties. It is relevant to investigate whether chemical surface treatment can increase adhesion properties. In addition, the surface topology can be investigated. Whether or not it is possible to rough the surface, or even to design and print a rougher surface on the gripper. In addition to increasing adhesion by chemical surface treatment, increasing the magnitude of local surface topology could increase the adhesion properties of the material.

One additional practical performance indicator of a soft gripper is the operation speed. The maximum operation speed without losing grip and force accuracy is relevant when using the gripper in practice. Analysis has not yet been executed on time-relevance. Several presented parameters are in fact dependent on the time parameter. For instance, the mechanical properties have been determined with a constant strain rate of 20 mm/min. When increasing the strain rate, properties such as hysteresis and ultimate elongation can be affected. When operating above the internal relaxation time scale the material may behave differently from the expectation based on this research. Therefore, this time-dependency in operation is a relevant property to further investigate.

Before producing this gripper to be used in practice, it is interesting to gather information about the lifetime of the gripper. The gripper material will be influenced by UV radiation, which is present in sunlight. Material parameters of the gripper are presumably affected by extended exposure to UV light. The material is formed by a specific intensity and exposure time of UV radiation. It is interesting to gather information on the influence for functional properties by additional UV exposure and whether this defines the lifetime of the gripper depending on the desired operation accuracy.

Small deviations in material properties can be compensated by adding sensing abilities to the gripper. By adding sensing abilities to the gripper a feedback system can be created. The possibility to measure the deformation ensures the gripper to be operated with the aimed force and deformation.

6.2 Implementation of strain sensors

Holst Centre is interested in continuing this research by integrating sensing abilities into the soft gripper. For instance, by implementing a strain sensor one can create a feedback system, in which the bending can be determined by measuring the strain of the bottom during operation. Holst Centre has investigated whether conductive ink adheres to the Elastic 50A material, showing decent results. Therefore it should be possible to print a conductive ink to create a strain sensor on the bottom of the gripper. The sensing accuracy required for measuring deformation of this gripper is analyzed shortly below.

If the strain sensor is printed at the bottom of the gripper, the bending movement decreases the length of the cured ink which subsequently decreases the resistance. This creates the ability to measure the deformation. To determine the properties of this sensor we should investigate the relation between deformation and the change in length of the sensor.

The relation between the deformation and the length at the neutral line is defined as shown in [Equation 9](#) where L is the neutral line length in [mm], R the bending radius in [mm], and θ the bending angle in [rad].

$$L = R \cdot \theta \quad (9)$$

The neutral line is assumed to be at height $H/2$, at this height the distance L is constant. It is assumed that the material behaves linear and analytical in compression and elongation. The length of the bottom line is $L - \delta L$, which is the length that the strain sensor will measure. The relation is stated as

$$L - \delta L = (R - H/2) \cdot \theta. \quad (10)$$

When [Equation 9](#) is subtracted from [Equation 10](#), the relation between δL and the deformation is obtained.

$$\delta L = \theta \cdot H/2 \quad (11)$$

If desired, this can be converted to the displacement x of the tip. R_b is introduced as the radius of curvature at the bottom, which is defined as $R_b = R - H/2$. x can be calculated by the following equation.

$$x = R_b \cdot (1 - \cos(\theta)) \quad (12)$$

The relation between the measurable value δL and the displacement x is of interest. This relation is depicted in [Figure 51](#), which is calculated for a rotation θ of 0 up to 90° .

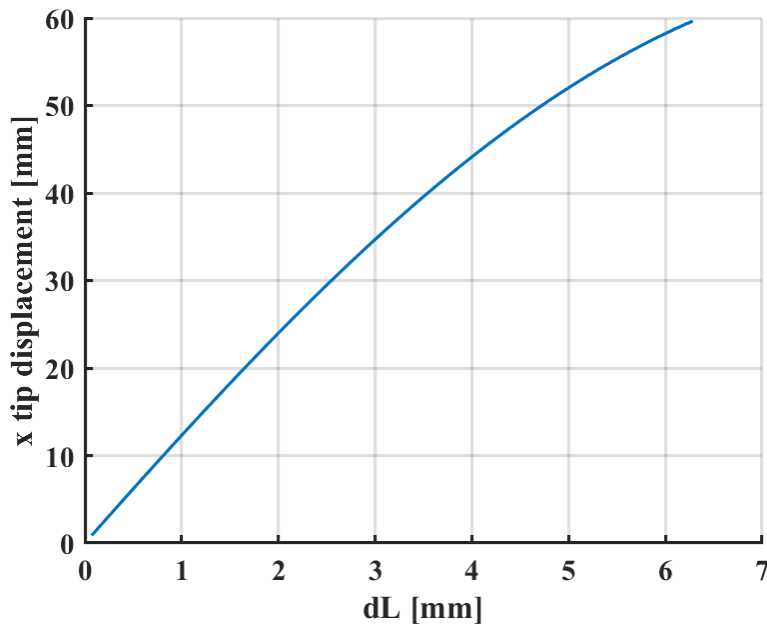


Figure 51: The relation between the tip displacement and the change in length of the bottom δL to be measured by the strain sensor, calculated from zero deformation up to 90° .

For instance, if we want to measure the displacement of the tip with an accuracy of a few millimeters, the accuracy of the strain sensor should be in the order of 0.1 mm. The total range of the sensor should be up to 10 mm without failure. To conclude, a strain sensor with a range of 10 mm with an accuracy of 1% is desired for measuring the deformation of the gripper.

6.3 Advanced actuation

As presented in [Subsection 4.5](#), the valve system can be improved. This research presented a proof of concept monolithic 3D-printed valve. This valve is able to close off and keep a system pressurized from 0.5 bar to 1 bar. To create advanced actuation possibilities for a gripper using valves, multiple valves have to be developed. In addition to the developed valve, a valve that is able to release the pressure from the system is necessary after the developed valve was able to close the system.

The valve is approximately 50 mm in size, which is too large compared to the developed gripper to be implemented in the body. If the 3D-printing technology develops further to higher resolutions, research can be conducted to investigate whether the current design of the valve is scalable to smaller dimensions.

A Appendix

A.1 Specimen thickness

Table 9: Measurement data for individual specimen thickness for the 24 specimens. For each specimen the measured points in millimeters are shown, along with the mean and 95% confidence interval.

Specimen	1	2	3	4	5	6	7	8	9	10	11	12
	2.74	2.77	3.06	2.82	2.83	2.76	2.83	2.82	2.70	2.79	2.77	2.92
	2.86	2.89	3.05	2.75	2.83	2.6	2.81	2.93	2.63	2.92	2.52	2.92
	2.72	2.73	3.02	2.70	2.96	2.72	2.84	2.75	2.65	2.80	2.7	2.79
	2.90	2.75	3.03	3.23	2.80	3.09	2.74	2.82	2.82	2.82	2.79	2.78
	2.87	2.87	2.92	2.76	2.74	2.87	2.76	2.75	2.65	2.75	2.79	2.82
	2.75	2.73	2.89	2.70	2.77	3.03	2.76	3.30	2.72	2.87	3.02	3.04
	2.79	2.76	2.92	2.74	2.84	3.12	2.74	2.88	2.73	3.05	2.89	2.90
	2.88	2.86	2.86	2.80	2.94	3.24	2.94	2.80	2.71	2.70	2.73	2.85
	2.90	2.79	2.76	2.80	2.78	3.16	2.76	2.92	2.75	2.72	2.83	2.81
	2.73	2.75	2.86	2.98	2.83	3.25	2.77	2.77	2.79	2.87	2.80	2.85
	2.70	2.75	2.70	2.86	2.84	3.06	3.07	3.00	2.54	3.13	2.80	2.94
	2.73	2.79	3.00	2.71	2.83	3.10	2.67	2.79	2.83	2.83	2.72	2.72
	2.74	2.69	2.72	2.92	2.70	2.37	2.66	2.67	2.65	2.90	2.67	2.58
	2.73	2.81	2.82	2.77	2.60	2.89	2.68	2.65	2.66	2.50	2.78	2.77
	-	-	-	2.80	2.74	2.98	2.86	2.81	2.65	2.74	2.67	2.74
	-	-	-	2.74	2.86	2.69	2.70	2.58	2.63	2.84	2.67	2.78
Mean	2.79	2.78	2.90	2.82	2.81	2.93	2.79	2.83	2.69	2.83	2.76	2.83
95% CI	0.145	0.112	0.234	0.26	0.169	0.482	0.206	0.32	0.15	0.278	0.214	0.207

Specimen	13	14	15	16	17	18	19	20	21	22	23	24
	2.60	2.66	2.83	2.75	2.71	2.65	2.65	2.55	2.88	2.66	2.68	2.73
	2.54	2.71	2.72	2.64	2.63	2.81	2.58	2.58	2.71	2.67	2.80	2.80
	2.64	2.70	2.70	2.72	2.66	2.61	3.07	2.65	2.94	2.74	2.61	2.46
	2.59	2.69	2.58	2.57	2.69	2.59	2.69	2.67	3.01	2.71	2.63	2.56
	2.60	2.72	2.58	2.56	2.54	2.59	2.67	2.48	2.92	2.63	2.94	2.71
	2.89	2.74	2.60	2.77	2.76	2.59	2.56	2.60	2.72	2.73	2.73	3.12
	2.73	2.75	2.64	2.66	2.60	2.54	2.74	2.66	2.69	3.03	2.60	2.92
	2.95	2.81	2.74	2.84	2.63	2.68	2.70	2.59	2.72	2.63	2.62	2.68
	2.36	2.87	2.72	2.65	2.65	2.59	2.63	2.75	2.65	2.75	2.71	2.74
	2.76	2.77	2.63	2.57	2.52	2.64	2.76	2.85	2.70	2.82	2.84	2.72
	2.64	2.67	2.63	2.55	2.74	2.66	2.74	2.75	2.80	2.91	2.88	2.79
	2.64	2.68	2.65	2.59	2.47	2.72	2.41	2.34	2.78	2.57	2.45	2.68
	2.58	2.67	2.50	2.56	2.51	2.76	2.60	2.28	2.68	2.50	2.68	2.55
	2.68	2.69	2.55	2.48	2.42	2.68	2.38	2.35	2.81	2.52	2.42	2.75
	2.83	2.75	2.53	2.56	2.48	2.48	2.58	2.30	2.47	2.60	2.65	2.94
	2.83	2.69	2.75	2.59	2.49	2.54	2.60	2.80	2.53	2.72	2.65	2.76
Mean	2.68	2.72	2.65	2.63	2.59	2.63	2.65	2.57	2.75	2.70	2.68	2.74
95% CI	0.286	0.111	0.178	0.188	0.201	0.165	0.3	0.351	0.277	0.266	0.269	0.308

A.2 Hysteresis

Table 10: Hysteresis calculated values for each cycle for each specimen. Presented with the mean value for each cycle and the 95% CI.

Specimen number	Cycle 5% ϵ_{eng}	Cycle 10% ϵ_{eng}	Cycle 20% ϵ_{eng}
1	2.625	2.444	1.366
2	3.519	2.007	1.166
3	4.048	2.198	1.227
4	2.843	2.343	1.251
5	3.067	2.444	1.164
6	2.702	1.670	0.760
7	3.835	1.849	0.809
8	3.350	1.951	1.067
9	2.659	2.083	1.013
10	3.576	1.467	0.959
11	2.309	2.255	0.911
12	3.253	2.154	1.162
13	3.684	1.739	0.843
14	3.276	2.232	1.027
15	2.443	2.339	1.256
Mean	3.146	2.079	1.065
95% CI	± 1.065	± 0.588	± 0.364

Table 11: Ultimate stress and true strain values obtained from measurement data. Affiliated stress-strain curves are presented in [Figure 52](#).

Specimen	Ultimate true strain [-]	Ultimate stress [MPa]
1	0.386	0.837
2	0.483	1.035
3	0.422	0.885
4	0.639	1.358
5	0.359	0.813
6	0.553	1.196
7	0.547	1.176
8	0.636	1.367
9	0.405	0.947
10	0.498	1.143
11	0.548	1.247
12	0.399	0.890
13	0.651	1.468
14	0.557	1.223
15	0.557	1.210
16	0.480	1.069
17	0.538	1.185
18	0.437	0.962
19	0.477	1.088
20	0.418	0.916
21	0.409	0.932
22	0.601	1.295
23	0.592	1.270

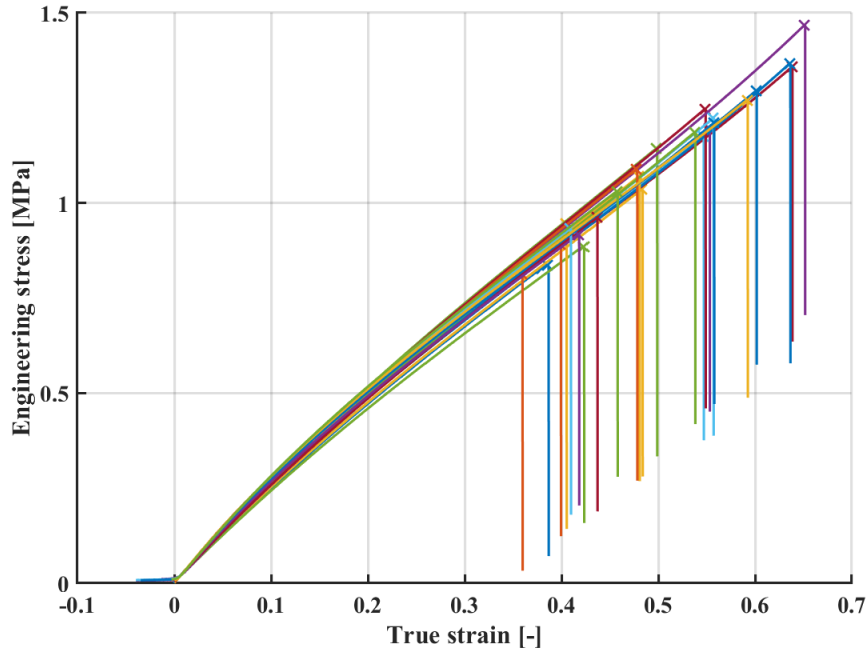


Figure 52: Stress-strain curve of the ultimate elongation measurement. Each line corresponds to a single specimen. The point of failure is indicated by an 'x'.

References

- [1] J. Shintake, V. Cacucciolo, D. Floreano, and H. Shea, “Soft robotic grippers,” *Advanced Materials*, vol. 30, no. 29, p. 1707035, 2018.
- [2] T. Hellebrekers, K. Ozutemiz, J. Yin, and C. Majidi, “Liquid metal-microelectronics integration for a sensorized soft robot skin,” pp. 5924–5929, October 2018.
- [3] T. Yamaguchi, T. Kashiwagi, T. Arie, S. Akita, and K. Takei, “Human-like electronic skin-integrated soft robotic hand,” *Advanced Intelligent Systems*, vol. 1, no. 2, p. 1900018, 2019.
- [4] F. Ilievski, A. D. Mazzeo, R. F. Shepherd, X. Chen, and G. M. Whitesides, “Soft robotics for chemists,” *Angewandte Chemie International Edition*, vol. 50, no. 8, pp. 1890–1895, 2011.
- [5] M. Wehner, R. Truby, D. Fitzgerald, B. Mosadegh, G. Whitesides, J. Lewis, and R. Wood, “An integrated design and fabrication strategy for entirely soft, autonomous robots,” *Nature*, vol. 536, pp. 451–455, August 2016.
- [6] D. K. Patel, A. H. Sakhaei, M. Layani, B. Zhang, Q. Ge, and S. Magdassi, “Highly Stretchable and UV Curable Elastomers for Digital Light Processing Based 3D Printing,” *Advanced Materials*, vol. 29, no. 15, pp. 1–7, 2017, ISSN: 15214095.
- [7] Formlabs, *Formlabs at CES Presents How 3D Printing is Changing The Way We Work*, 2019. [Online]. Available: <https://formlabs.com/company/press/formlabs-at-ces-presents-how-3d-printing-is-changing/> (visited on 12/03/2020).
- [8] Formlabs, *Elastic 50A Resin 1 L*. [Online]. Available: <https://formlabs.com/store/elastic-resin/> (visited on 12/03/2020).
- [9] T. J. Wallin, J. Pikul, and R. F. Shepherd, “3D printing of soft robotic systems,” *Nature Reviews Materials*, vol. 3, no. 6, pp. 84–100, 2018, ISSN: 20588437.
- [10] E. Sachyani Keneth, A. Kamyshny, M. Totaro, L. Beccai, and S. Magdassi, “3d printing materials for soft robotics,” *Advanced Materials*, vol. 33, no. 19, p. 2003387, 2020.
- [11] H. M. C. M. Anver, R. Mutlu, and G. Alici, “3d printing of a thin-wall soft and monolithic gripper using fused filament fabrication,” pp. 442–447, 2017.
- [12] R. Mutlu, S. K. Yildiz, G. Alici, M. in het Panhuis, and G. M. Spinks, “Mechanical stiffness augmentation of a 3d printed soft prosthetic finger,” pp. 7–12, 2016.
- [13] H. K. Yap, H. Ng, and R. C.-H. Yeow, “High-force soft printable pneumatics for soft robotic applications,” *Soft Robotics*, vol. 3, pp. 144–158, Sep. 2016.
- [14] B. A. W. Keong and R. Y. C. Hua, “A novel fold-based design approach toward printable soft robotics using flexible 3d printing materials,” *Advanced Materials Technologies*, vol. 3, no. 2, p. 1700172, 2018.
- [15] S. Dilibal, H. Sahin, J. O. Danquah, M. O. F. Emon, and J.-W. Choi, “Additively manufactured custom soft gripper with embedded soft force sensors for an industrial robot,” *International Journal of Precision Engineering and Manufacturing*, vol. 22, no. 4, pp. 709–718, 2021.
- [16] Y. L. Yap, S. L. Sing, and W. Y. Yeong, “A review of 3D printing processes and materials for soft robotics,” vol. 8, pp. 1345–1361, 2020.
- [17] R. L. Truby and J. A. Lewis, “Printing soft matter in three dimensions,” *Nature*, vol. 540, no. 7633, pp. 371–378, 2016, ISSN: 14764687.
- [18] F. Jan, J. Glowka, and K. Althoefer, “Instant soft robot: A simple recipe for quick and easy manufacturing,” pp. 482–488, May 2020.
- [19] B. N. Peele, T. J. Wallin, H. Zhao, and R. F. Shepherd, “3d printing antagonistic systems of artificial muscle using projection stereolithography,” *Bioinspiration & biomimetics*, vol. 10, no. 5, p. 055003, 2015.
- [20] W. Dou, G. Zhong, J. Cao, Z. Shi, B. Peng, and L. Jiang, “Soft robotic manipulators: Designs, actuation, stiffness tuning, and sensing,” *Advanced Materials Technologies*, vol. n/a, no. n/a, p. 2100018, 2021.
- [21] Distrilec, *SOFT ROBOTICS GRIPPER KIT - mGrip P2 Robot Gripper Kit, 8N, Fingers 2, Soft Robotics*. [Online]. Available: <https://www.distrielec.nl/nl/mgrip-p2-robot-gripper-kit-8n-fingers-soft-robotics-soft-robotics-gripper-kit/p/30185725> (visited on 08/09/2021).

- [22] S. R. inc., *The mGrip™ Modular Gripping System*. [Online]. Available: <https://www.softroboticsinc.com/products/mgrip-modular-gripping-solution-for-machine-builders/> (visited on 08/09/2021).
- [23] Z. Wu, X. Li, and Z. Guo, "A novel pneumatic soft gripper with a jointed endoskeleton structure," *Chinese Journal of Mechanical Engineering*, vol. 32, no. 1, pp. 1–12, 2019.
- [24] B. Mosadegh, C. Kuo, Y. Tung, Y.-s. Torisawa, and S. Takayama, "A monolithic passive check-valve for systematic control of temporal actuation in microfluidic devices," vol. 1216, p. 826 828, 2008.
- [25] M. A. Unger, H.-P. Chou, T. Thorsen, A. Scherer, and S. R. Quake, "Monolithic microfabricated valves and pumps by multilayer soft lithography," *Science*, vol. 288, no. 5463, pp. 113–116, 2000.
- [26] R. Walczak, K. Adamski, and D. Lizanets, "Inkjet 3d printed check microvalve," *Journal of Micromechanics and Microengineering*, vol. 27, no. 4, p. 047002, 2017.
- [27] A. Zatopa, S. Walker, and Y. Menguc, "Fully soft 3d-printed electroactive fluidic valve for soft hydraulic robots," *Soft robotics*, vol. 5, no. 3, pp. 258–271, 2018.
- [28] S. Ltd., *Digital materials data sheet*. [Online]. Available: https://www.stratasys.com/-/media/files/material-spec-sheets/mss_pj_digitalmaterialsdatasheet_0617a.pdf (visited on 06/16/2021).
- [29] Formlabs, *Using elastic 50a resin*. [Online]. Available: https://support.formlabs.com/s/article/Using-Elastic-Resin?language=en_US#comparison (visited on 06/24/2021).
- [30] Instron, *Series 5560 standard model specifications*. [Online]. Available: <https://www.equipx.net/uploads/Instron/Instron5560seriesSpecifications.pdf> (visited on 06/29/2021).
- [31] Mark-10, *Model 7i professional force/torque indicator*. [Online]. Available: <https://mark-10.com/products/indicators-sensors/indicators/model-7i/> (visited on 07/09/2021).
- [32] Mark-10, *Series r03 tension and compression force sensors*. [Online]. Available: <https://mark-10.com/products/indicators-sensors/force-sensors/r03/> (visited on 07/09/2021).
- [33] R. T. Fenner and J. Reddy, *Mechanics of solids and structures*. CRC Press/Taylor & Francis Group, 2012, ISBN: 9781439858141.

Declaration concerning the TU/e Code of Scientific Conduct for the Master's thesis

I have read the TU/e Code of Scientific Conduct¹.

I hereby declare that my Master's thesis has been carried out in accordance with the rules of the TU/e Code of Scientific Conduct

Date

13/09/2021


Name

Roel de Groot

ID-number

0913359

Signature



Submit the signed declaration to the student administration of your department.

¹ See: <http://www.tue.nl/en/university/about-the-university/integrity/scientific-integrity/>

The Netherlands Code of Conduct for Academic Practice of the VSNU can be found here also.
More information about scientific integrity is published on the websites of TU/e and VSNU